EMBRY-RIDDLE
Aeronautical University™
SCHOLARLY COMMONS

Spring 4-2016

Oscillatory Flow Mechanism for Enhanced Heat Transfer

Sultan Taher Raml
Embry-Riddle Aeronautical University

Follow this and additional works at: https://commons.erau.edu/edt

Part of the Heat Transfer, Combustion Commons

OSCILLATORY FLOW MECHANISM FOR ENHANCED HEAT TRANSFER

By

Sultan Taher Raml

A Thesis Submitted to the College of Engineering Department of Mechanical Engineering in
Partial Fulfillment of the Requirements for the Degree of Master of Science in Mechanical
Engineering

Embry-Riddle Aeronautical University

Daytona Beach, Florida

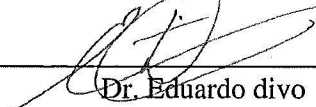April/2016

Thesis Review Committee

OSCILLATORY FLOW MECHANISM FOR ENHANCED HEAT TRANSFER

by

Sultan Taher Raml

This thesis was prepared under the direction of the candidate's Thesis Committee Chair, Dr. Eduardo Divo, Professor, Daytona Beach Campus, and Thesis Committee Members Dr.Sandra Boetcher , Professor, Daytona Beach Campus, and Dr. Ilteris Demiirkiran, Professor, Daytona Beach Campus, and has been approved by the Thesis Committee. It was submitted to the Department of Mechanical Engineering in partial fulfillment of the requirements for the degree of Master of Science in Mechanical Engineering
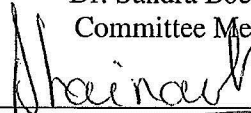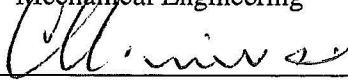
Thesis Review Committee:

_____
Dr. Eduardo divo
Committee Chair

_____
Dr. Sandra Boetcher.
Committee Member

_____
Jean-Michel Dhainaut, Ph.D.
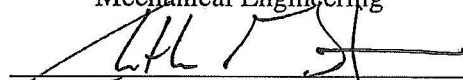Graduate Program Chair,
Mechanical Engineering

_____
Maj Mirmirani, Ph.D.
Dean, College of Engineering

_____
Dr. Ilteris Demiirkrian
Committee Member

_____
Charles F. Reinholtz, Ph.D.
Department Chair,
Mechanical Engineering

_____
Christopher Grant, Ph.D.
Associate Vice President of Academics

_____
Date

i

Abstract

Researcher: Sultan Taher Raml

Title: Oscillatory Flow Mechanism for Enhanced Heat Transfer

Institution: Embry-Riddle Aeronautical University

Degree: Master of Science in Mechanical Engineering

Year: 2016

This research project is about the use of an oscillatory flow mechanism to enhance heat transfer. The idea behind this is to induce oscillation of the end wall of one of two connected chambers of a heat exchanger which effectively will induce oscillation of the boundary layer within the connecting duct. The main idea of this thesis came from using species separation studies before 40 years ago in hyperventilation technology to help patients under anesthesia in hospitals. There are many applications for this research such as removing heat from chemical reactors, electrical devices and other enclosed environments such as submarines, underground facilities and so forth. Many parameters can be varied to maximize the convective heat transfer. These parameters include the amplitude and frequency of oscillation, as well as duct radius and length.

In this thesis, results from three-dimensional time-accurate studies carried out using computational fluid dynamics are presented. These results simulate the diffusion and convection of energy in air. The model consists of two chambers with inlets at two different temperatures, an oscillating piston wall on one of the chambers, and a connecting tube. Several cases are carried out reporting on heat transfer enhancement as a function of the tidal displacement to connecting tube diameter. Unlike previous studies which were undertaken using asymptotic analysis, the

present models and results incorporate full entrance effects and 3D interactions. Results of this study will be useful as a guide for the design and miniaturization of an oscillating device for enhanced heat transfer in further research projects.

Simulations were performed to analyze the effect of oscillations on the heat transfer. A simulation was first carried out in steady-state to serve as the baseline for comparison with time-accurate oscillating results. The remaining simulations consist of altering the frequency and tidal displacement of the moving wall to analyze their effect on the heat transfer between the two chambers. The results suggest that the heat transfer is enhanced as a function of the frequency and tidal displacement of the moving wall and that there should be an optimal point. Results are presented in the form of contour and vector plots of the temperature and velocity fields as well as plots of the heat exchanger outlet temperatures as a function of frequency and displacement.

List of Contents

List of Tables

List of Figures

x

List of Abbreviations

C_p Specific heat at constant pressure, J/kg K

D   Diameter of the cylinder, device, m

D_T Thermal diffusion coefficient, m^2/s

G   Mass Flux, or mass velocity, ρ .V

H   Heat transfer coefficient, or convection conductance, W/m^2.k

K_T Thermal diffusion ratio, D_T/D_j

L   Length of the cylinder, m

Q   Heat Flux, heat- transfer rate at surface per unit area, W/m^2

Q   Mass transfer rate, kg/s

R   Radius of the cylinder, also found as a in 1-d equations, m

V   Axial velocity vector, m/s

v   Velocity magnitude, m/s

ρ Fluid density, kg/m^3

p   Pressure

g   Gravity

$\vec{f}$ Applied force per unit volume on fluid particle

Δt	Time step
$\vec{F}$	Force vector
τ	Shear stress
τ_{ij}	Stress Tensor
T	Temperature (K)
2D	Tow-dimensions
3D	Three-Dimensions
CFD	Computational Fluid Dynamic

CHAPTER I

Introduction

This research is about the use of an oscillatory flow mechanism to enhance heat transfer. The idea behind this is inducing the oscillation at the end wall of one of two connected chambers of a heat exchanger which effectively will induce oscillation of the boundary layer within the connecting duct. It is proposed to study a novel method for the enhanced heat removal from an enclosed system. Enhanced heat removal is needed when high heat generation occurs as in power generation systems, operation of fuel cells, power cycles and even in materials processing. Removal of this heat is important for proper thermal control for human habitation and instruments in an extra-terrestrial space environment. Such technology also has spin-off uses in Earth applications as in the thermal stability of chemical reactors, removal of heat from electrical devices and other enclosed environments such as submarines, underground facilities and so forth.

Removal of heat from confined cabins and space habitats is of immense importance to many applications in order to ensure proper thermal control. Currently, many of the thermal subsystems involve single-phase fluid and heat transfer processes; but the need for improved energy-to-mass ratios and the availability of future spacecraft that will generate large quantities of power and waste energy, such as the nuclear based ones, is urging a shift towards two-phase operations. Consequently, the design of important thermal subsystems for future applications as in boilers, condensers, evaporators, heat exchangers, phase separators, normal and cryogenic fluid storage units, fuel cells, radiators, and heat pipes will all involve complex multiphase fluid flow and transport microgravity issues. There is a real and immediate need for both basic research and engineering development in this area.

Creating a three-dimensional computational fluid dynamics (CFD) model to simulate an oscillatory flow driven by piston motion is the main purpose of this thesis. This model simulates a physical device that consists of two chambers connected by a cylindrical duct. This thesis studies how the time accurate CFD simulation incorporates entrance and exit effects as well as three dimensionality of the problem using a trimmed grid replicating most of the structure of the device while the pulsatile motion is imparted by a sinusoidal moving wall in one of the reservoirs.

Initially, the time-accurate CFD model is ran through the steady state regime until it reaches convergence. Then the moving wall is initialized to make the CFD model the transient regime. The results are analyzed after a periodic sustained regime is reached. The main purpose of this approach is to compare heat transfer obtained between the steady state regime and the oscillatory flow driven by the motion of the wall (piston).

Comparisons are made for several values of amplitudes of piston's movement to provide a guide for design and implementation of physical devices. The commercial code STAR-CCM+ (from CD-Adapco) was used for all CFD modeling. The 3-D time-accurate CFD study reveals improvement in the heat transfer under oscillatory motion, confirming theoretically predicted results.

CHAPTER II

Theoretical Background

2.1 Background

Many researchers have studied the oscillatory flow mechanism by using transfer of energy method. A new technology has been developed for the heat transfer enhancement by sinusoidal oscillation of a fluid by Kurzweg [1-3]. This technology showed that highly enhanced by imposing sinusoidal oscillation took place in a pipe connecting to hot and cold reservoirs at both ends. Also, using oscillatory flow techniques can enhance the forced convection heat transfer in tubes [4-6].

In Addition, removal heat from the steam engine and turbine was the big issue that engineers faced. Consequently, many studies and experimental designs of heat pipes started growing after recognizing the heat pipe as an important development in heat transfer technology such as what Kurzweg and Zhao developed in (1984) [1].

Moreover, many different studies from the more recent investigations of Chatwin [7], Kurtweg [8], Wastson [9], and Jaeger [10], as well as Taylor [11] showed that there is dispersing for contaminants or gas constituents in both steady and oscillatory viscus laminar flows within pipes at rates much higher than suggested on pure molecular diffusion grounds. It was proved that the interaction of the cross-stream-dependent viscus velocity distribution and the radially dependent could produce enhanced diffusion in flows from side where there is high concentration to other with low concentration. From their studies, Kurzweg and Jeager recognized "that there should be an equivalent enhanced diffusion process occurring in the area of heat transfer because of similarity between the diffusion and heat conduction equations" [8].

In this thesis, the idea of enhanced heat transfer by using an oscillatory flow mechanism. Unlike the studies of separation of species of axial dispersion in steady flows that investigated the phenomenon of transport enhancement of species, heat transfer in this thesis happens by the transfer of energy. Heat transfer transfers from hot reservoir to cold reservoir either by normal conduction if there is no an external force (piston) or by both forced convection and normal conduction if oscillation is applied.

Although there is a difference between mass transfer and energy transfer in applying, the principle of diffusion is still the same and only it can been described by the equation of energy and the equation of mass transfer. The idea behind this thesis can be traced back to hyperventilation studies done over 40 years ago and to the implementation of the technology in hospital environments to provide life-support for patients under anesthesia. However, it is only in recent years that the underlying physics of oscillatory flow as applied to heat transfer are being understood. This has given the opportunity to apply this technique to novel means of enhancing heat transfer by as much as 20,000 times over molecular conduction without the use of metals which are typically quite heavy. The phenomenon of transport enhancement of contaminants was initially investigated by Taylor [11] and Aris [12] in studies of axial dispersion in steady flows. It is from these results that we learn that heat transfer can be enhanced substantially.

The idea of the proposed technology is based upon a) our current experience on enhanced mass transfer using oscillatory flow and b) theoretical work done by Kurzweg and co-workers at the Univ. of Florida. The idea is to enhance the heat transport substantially beyond thermal conduction. Imagine a connecting pipe between the left and right tanks containing fluid. This fluid is merely a carrier of heat from left to right tanks. If there were no motion in the fluid then heat

4

will transfer by molecular conduction. If the fluid were deliberately set into oscillatory motion then a sharp spike in the profile will be created as the fluid moves from left to right. The sharp spike in the velocity profile generates more area for heat transfer and allows heat to diffuse from the core to the boundary. In the reverse cycle the heat from the boundaries (which are ordinarily insulated to heat) diffuse to the cooler core and the process continues where the heat moves in a zig-zag fashion from the source tank to the sink tank. This method can enhance the heat transfer by as much as 20,000 times or more than molecular conduction. Moreover there is no net flow between the reservoirs. The heat sink can be a heat pipe or it can be external radiators. This technique could therefore be used in connection with a heat pipe or, in some instances, become a replacement for heat pipes. The energy required for pumping the flow is calculated to be about 10-5 times the neat transferred and this is virtually insignificant given the advantage of quick and large removal of heat. With proper engineering architecture the mechanism for oscillations can be hooked onto a fly-wheel from existing motors on board thus eliminating the need for added mass. The materials of construction of the device can be made of light weight composites and depending upon the working temperatures the working fluid can be water or silicone oils. For high temperature applications other fluids may be used.

2.2 Governing equations

2.2.1 The Navier-Stokes Equations

The Navier-stokes equations were developed by Claude-Louis Navier and George Gabrial Stokes before almost 200 years ago. These equations can be used to determine the velocity vector field that applies to a fluid. Newton's second law was the main source for these equations and they grow from its applications in combination with a fluid stress (due to viscosity) and a pressure term. Navier-stokes equations are almost nonlinear partial equations in all real situations, but they can be reduced to linear equations with certain simplifications such as 1-dimensional motion. However, the main problem to solve them when they are nonlinear and this situation makes them very difficult and impossible to solve [13].

From the basic conservation and continuity equations that apply to properties of fluids, the Navier-Stokes can be derived. To combine the conservation equations with a physical understanding of what a fluid is, the continuity equation should be derived first and the equation of fluid motion second.

The remaining section shows steps to derive Navier-Stokes equations to get the form of general Navier-Stokes equations. The continuity equation defines the change of an intensive property L, a property independent of the amount of material that researchers have. There are some examples for intensive and extensive property, such as temperature and heat, but temperature would be an intensive property while heat would be the corresponding extensive property. In addition, it is assumed that the volume Ω is any form and its bounding surface area is indicated as $\partial\Omega$.

6

After giving a short explanation about continuity equation, Reynold's Transport Theorem is ready to be derived. From the equation of the rate of change of the property L which contains inside volume Ω, Reynold's Transport Theorem can be obtained from the both terms on the right side: a flux term, $\int_{\partial\Omega} L.\vec{v}.\vec{n}\, dA$, which represents the amount of the flowing property L over the boundary $\partial\Omega$ from the volume, and a sink term, $\int_{\Omega} Q\, dV$, which defines how much the leaving property L from the volume because of the sinks or sources inside the boundary. As shown below in equation (1):

$$\frac{d}{dt}\int_{\Omega} L\, dV = -\int_{\partial\Omega} L.\vec{v}.\vec{n}\, dA - \int_{\Omega} Q\, dV \tag{1}$$

The flux term can be expressed as a volume integral according to the divergence theorem:

$$\int_{\partial\Omega} L.\vec{v}.\vec{n}\, dA = \int_{\Omega} \nabla.(L.\vec{v})\, dV \tag{2}$$

As a result, the equation (1) can be written in a new form:

$$\frac{d}{dt}\int_{\Omega} L\, dV = -\int_{\Omega} \nabla.(L.\vec{v}) + Q\, dV \tag{3}$$

In addition, from the equations above and by applying Leibniz's Rule, the general form of the continuity equation will be easy to obtain. The Leibniz's rule states that

$$\frac{d}{dx}\int_{a}^{b} f(x,y)\, dy = \int_{a}^{b} \frac{d}{dx} f(x,y) \tag{4}$$

By applying the rule of equation (4) in equation (3), it shows that

$$\int_{\Omega} \frac{d}{dt} L\, dV = -\int_{\Omega} \nabla.(L\vec{v}) + Q\, dV \tag{5}$$

Equivalently,

$$\int_{\Omega} \frac{d}{dt} L\, dV + \nabla.(L\vec{v}) + Q\, dV = 0 \tag{6}$$

7

Finally, to any control volume Ω, this relation can be applied and in accordance with the condition that says if the integrand itself is zero, this equality remains true for all control volumes. Therefore, the general form of continuity equation is

$$\frac{dL}{dt} + \nabla \cdot (L\vec{v}) + Q = 0 \qquad (7)$$

In this thesis, Navier-Stokes equations are studied with incompressible viscous flow in the laminar regime. However, for a physical system to be considered conservative, it must follow three laws of conservation: conservation of mass (continuity equation), conservation of momentum (Newton's second law), and conservation of energy (the first law of thermodynamics). From these three equations, velocity ($\vec{v}$), pressure (p), absolute temperature (T), density (ρ), enthalpy (h), the dynamic viscosity (μ), and the heat transfer coefficient (k) can be obtained. Density, enthalpy, dynamic viscosity, and the heat transfer coefficient are all functions of the pressure and density. They are represented by the following equations [23]:

$$P = \rho\,(p, T) \qquad\qquad h = h\,(p, T) \qquad\qquad (8)$$

$$\mu = \mu\,(p, T) \qquad\qquad k = k\,(p, T) \qquad\qquad (9)$$

2.2.1.1 Conservation of Mass

The conservation of mass equation can be obtained by applying the continuity equation to density (the intensive property equivalent to mass):

$$\frac{dp}{dt} + \Delta \cdot (\rho\vec{v}) + Q = 0 \qquad (10)$$

But (Q= 0) because there are no sources or sinks of mass. The conservation of mass equation becomes:

$$\frac{dp}{dt} + \Delta \cdot (\rho\vec{v}) = 0 \qquad (11)$$

8

In this thesis, the mass is assumed to not be added or removed from the system. According to the incompressibility of fluids, the density remains constant. The simple form of mass equation can be obtained after setting the derivative of density equal to zero and dividing through by a constant ρ:

$$\nabla \cdot \vec{v} = 0 \tag{12}$$

2.2.1.2 Conservation of Momentum

The equation of the conservation of momentum has some materials which should be derived before deriving the momentum's equation. The first derivative is the rate of change of an intensive property at a point. For example, the rate of change of temperature at point (x, y) could be the value $\frac{dT}{dt}$ while the rate of change of an intensive property on a particle in a velocity field can be the second derivative in this part. The last material must combine two things: rate of change of the property, $\frac{dL}{dt}$, and change in position of the other particle in the velocity field $\vec{v}$. Therefore, the equation below can be obtained after deriving the material derivative:

$$\frac{Du}{Dt} = \frac{du}{dt} + (\vec{v} \cdot \nabla)\, u \tag{13}$$

The directional derivative of u in the direction of the velocity $\vec{v}$ can be represented by the expression $(\vec{v} \cdot \nabla)\, u$.

Here, the equation of momentum can be derived according to the previous information of the material derivatives. The rigorous derivation of the conservation of momentum equations can be achieved using Newton's laws and an application of the chain rule. The relation between an applied force and the resulting acceleration of a particle of mass m:

$$\vec{F} = m\, \vec{a} \tag{14}$$

9

By replacing $\vec{F}$ by $\vec{b}$ and substituting density for mass, the equation will be as shown below

$$\vec{b} = \rho \frac{d}{dt} \vec{v}(x, y, z, t) \tag{15}$$

The chain rule can be applied here to the derivative of velocity to get

$$\vec{b} = \rho \left(\frac{\partial \vec{v}}{\partial t} + \frac{\partial \vec{v}}{\partial x} \frac{\partial x}{\partial t} + \frac{\partial \vec{v}}{\partial y} \frac{\partial y}{\partial t} + \frac{\partial \vec{v}}{\partial z} \frac{\partial z}{\partial t} \right) \tag{16}$$

Equivalently,

$$\vec{b} = \rho \left(\frac{\partial \vec{v}}{\partial t} + \vec{v}. \nabla \vec{v} \right) \tag{17}$$

The final equation can be written in the formula below after substituting the value in parentheses for the definition of a material derivative

$$\rho \frac{D\vec{v}}{Dt} = \vec{b} \tag{18}$$

2.2.1.3 Equation of Motion

From the conservations equations derived above, the equations of motion for fluids can be obtained when some assumptions of the forces and the behavior of fluids are applied. For instance, there are two components for body force on the fluid parcels, fluid stress and external forces.

$$\vec{b} = \nabla. \sigma + \vec{f} \tag{19}$$

Where,

- σ: the stress tensor

- $\vec{f}$: external force

In addition, because the divergence is the extent to which the tensor acts like a sink or source, the divergence of the stress represents the fluid stress. On the other hand, a force that results in a momentum source or sink can be known as the divergence of tensor too.

10

2.2.1.4 Stresses

The stress tensor σ can be represented as shown below and it is very important for the

equations of motion because they depend on the stress of tensor.

$$\sigma = \begin{pmatrix} \sigma_{xx} & \tau_{xy} & \tau_{xz} \\ \tau_{yx} & \sigma_{yy} & \tau_{yz} \\ \tau_{zx} & \tau_{zy} & \sigma_{zz} \end{pmatrix} \tag{20}$$

In general, "a tensor is the concept of the higher-order quantity; a vector is represented as

first order tensor, a matrix as a second order tensor, a 3D matrix is a third order tensor
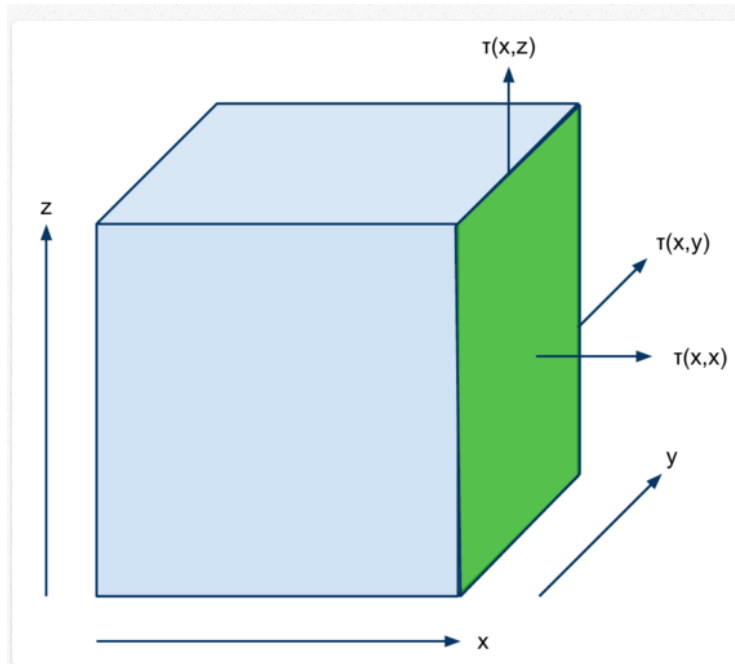
Figure 1: National for stresses

2.2.1.5 General form of the Navier-stokes equation

The stress tensor σ contains two terms in the general form of the Navier-Stokes equation.

The two terms are the the volumetric sterss tensor and steress deviator tensor. The volume body is

changed by the volumetric stress tensor while the the body is deformed by the stress deviator

tensor. For example, pressure forces that set the volume of the body is represented by the

11

volumetric stress tensor. Morever, represeinting the forces that find the deformaton and movment of the body is done by the stress deviator tensor. Then σ is broken down into

$$\sigma = \begin{pmatrix} \sigma_{xx} & \tau_{xy} & \tau_{xz} \\ \tau_{yx} & \sigma_{yy} & \tau_{yz} \\ \tau_{zx} & \tau_{zy} & \sigma_{zz} \end{pmatrix}$$

$$= - \begin{pmatrix} p & 0 & 0 \\ 0 & p & 0 \vdots \\ 0 & 0 & p \end{pmatrix} + \begin{pmatrix} \sigma_{xx} + p & \tau_{xy} & \tau_{xz} \\ \tau_{yx} & \sigma_{yy} + p & \tau_{yz} \\ \tau_{zx} & \tau_{zy} & \sigma_{zz} + p \end{pmatrix} \tag{20}$$

By showing the stress deviator tensor as T, the equation (20) can be substitution as shown below

$$\sigma = - PI + T \tag{21}$$

The general form of the Navier-Stokes equation can be written after substituting equation (21) into previous equation.

$$\rho \frac{D\vec{v}}{Dt} = - \nabla p + \nabla . T + \vec{f} \tag{22}$$

Note: this equation cannot be applied until it has been more specified. For instance, an expression must be determined for the stress tensor T depending on the type of the fluid. Also, an equation of state and an equation dictating conservation of energy are necessary if the fluid is not assumed to be incompressible.

2.2.1.6 Fluid Stress

The assumption about the nature of the stress tensor is the fundamental for Newtonian fluid equations that assumes the fluid is incompressible. The change in the velocity in the directions of the stress is represented by the rate of deformation that is proportional with stress for Newtonian fluid.

$$\tau_{ij} = \mu \left(\frac{\partial u_i}{\partial x_j} + \frac{\partial u_j}{\partial x_i} \right) \tag{23}$$

Where; μ is the viscosity of the fluid.

12

2.2.1.7 Stress Divergence

The Navier-Stokes equation uses the divergence of the stress, $\nabla \cdot T$. The stress term can be calculated as shown.

$$\nabla \cdot \sigma = \mu \, \nabla \cdot \begin{pmatrix} \sigma_{xx} & \tau_{xy} & \tau_{xz} \\ \tau_{yx} & \sigma_{yy} & \tau_{yz} \\ \tau_{zx} & \tau_{zy} & \sigma_{zz} \end{pmatrix}$$

$$= \mu \begin{pmatrix} 2\frac{\partial u}{\partial x} & \frac{\partial u}{\partial y}+\frac{\partial v}{\partial x} & \frac{\partial u}{\partial z}+\frac{\partial w}{\partial x} \\ \frac{\partial u}{\partial y}+\frac{\partial v}{\partial x} & 2\frac{\partial u}{\partial y} & \frac{\partial v}{\partial z}+\frac{\partial w}{\partial y} \\ \frac{\partial u}{\partial z}+\frac{\partial w}{\partial x} & \frac{\partial v}{\partial z}+\frac{\partial w}{\partial y} & 2\frac{\partial w}{\partial y} \end{pmatrix} \tag{24}$$

X term of the divergence can be calculated:

$$(\nabla \cdot \sigma)_i = \mu \frac{\partial}{\partial x}(2\frac{\partial u}{\partial x}) + \frac{\partial}{\partial y}(\frac{\partial u}{\partial y}+\frac{\partial v}{\partial x}) + \frac{\partial}{\partial z}(\frac{\partial u}{\partial z}+\frac{\partial w}{\partial x})$$

$$= \mu \frac{\partial^2 u}{\partial x^2} + \frac{\partial^2 u}{\partial y^2} + \frac{\partial^2 u}{\partial z^2} + \frac{\partial^2 v}{\partial x \partial y} + \frac{\partial^2 w}{\partial x \partial z}$$

$$= \mu \, \nabla^2 u + \mu \frac{\partial}{\partial x}(\frac{\partial u}{\partial x}+\frac{\partial v}{\partial y}+\frac{\partial w}{\partial z})$$

$$= \mu \, \nabla^2 u + \mu \frac{\partial}{\partial x}(\nabla \cdot v)$$

$$= \mu \, \nabla^2 u + 0$$

$$= \mu \, \nabla^2 u. \tag{25}$$

Replacing the divergence with a vector Laplacian:

$$\nabla \cdot T = \mu \, \nabla^2 \, v \tag{26}$$

2.2.1.8 Newtonian Fluid Equation

The final equation for an incompressible Newtonian fluid is:

$$\rho \frac{Dv}{Dt} = -\nabla p + \mu \nabla^2 v + f. \tag{27}$$

2.8 Conservation of Energy

The modified form of the first law of thermodynamics applied to an element of fluid states that the rate of change in the total energy (intrinsic plus kinetic) of the fluid as it flows is equal to the sum of the rate at which work is being done on the fluid by external forces and the rate on which heat is being added by conduction.

$$\rho c \frac{\partial T}{\partial t} + \rho c \, (\vec{V} . \nabla) \, T = k\nabla^2 \, T \tag{28}$$

2.3 Boundary Conditions

The reference values that defined in this part called the boundary conditions.

- The pulsating motion is governed by the following function:

$$X(t) = A_o \sin(\omega t) \tag{29}$$

- Therefore, the corresponding derivative in time yields the speed as:

$$V(t) = A_o \, \omega \cos(\omega t) \tag{30}$$

- Constant Properties:

- Specific Heat: c_p = 1003.62 (J/kg K)

- Thermal conductivity, k = 0.0260305 (W/mK)

- Dynamic viscosity, μ = 1.85508e-05 (kg/m s)

- Range of frequencies: f = 0.1 to 1.6 Hz

14

- Range of amplitudes, A_o = 5%, 7% and 10% of the length of the cylinder, which has a constant value of 1.34 m.

It can be seen clearly from the previous research that this topic is very important to get guides to narrow the range of the frequencies and amplitudes to be considered [16]. Results of the amplitudes vary according to cross-section area of the oscillating surface.

2.4 Time- changing domain

During the whole unsteady process, there were 48 cases with different amplitudes and frequencies tested by using the dynamic mesh model. Also, three amplitudes were chosen which were 5%, 7%, and 10% of the total length of the cylinder (1.34m). These percentages were applied on an oscillatory wall to ensure the right movement for the piston. It can be seen in the figure (2).
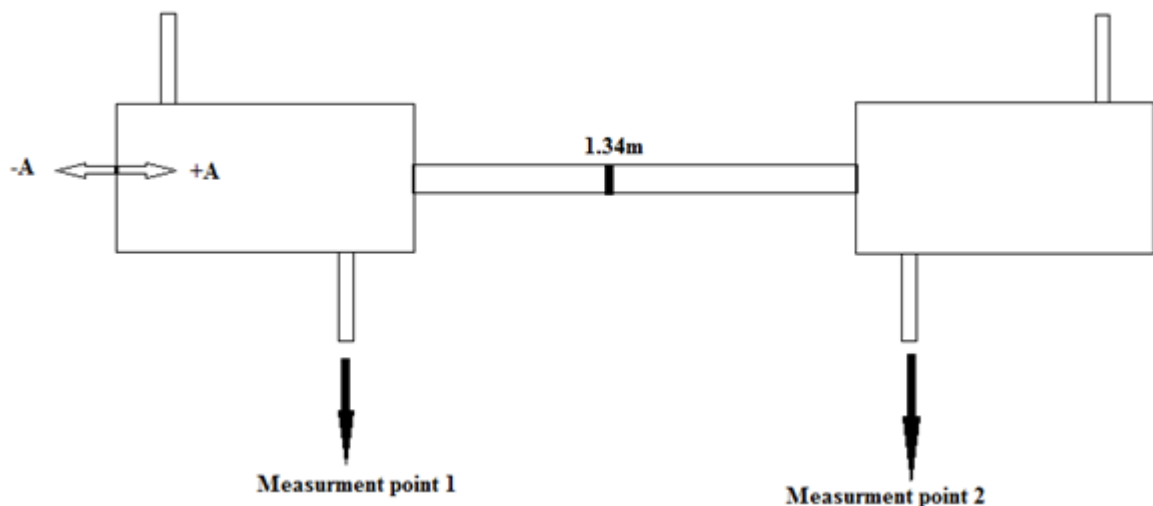

Figure 2: 2-D Sketch – Piston Wall - Amplitude Calculation

The frequencies vary from 0.1 Hz to 1.6 Hz for each amplitudes. For example, for 5%, 16 simulations were ran with frequencies from 0.1 to 1.6 Hz, and the situation was the same with the other amplitudes.

15

The primary results at the beginning of the challenge were very different from which were predicted, but many cases were tested to get the acceptable results. For instance, many frequencies were chosen before choosing the range from 0.1 to 1.6 Hz. As a result, high diffusion of energy was expected to transfer to make this thesis successful. The validation of results will be achieved when

- Total heat transfer increases with increasing ω

- Increasing the temperature at measurement point 2 while decreasing the temperature point 1 by choosing the right frequency and amplitude.

- Existence of optimal frequency and time-step.

For getting the right temperatures, two measurement points were chosen. The first one was at outlet 1 in the left-hand reservoir, and the second at outlet 2 in the right-hand reservoir.

There were many simulations tested (more than 120 simulations) by choosing different frequencies and amplitudes as well as time-steps. For example, at the beginning, 0.001s for the time-step was chosen with 0.1Hz and 5% L. This time-step was unsuccessful because it didn't give enough fast movement to the piston to make high diffusion. Therefore, it was a challenge to choose the right time-step. For instance, when the solver was set up with 0.001s for the time-step, the temperatures at outlet 1 and outlet 2 were very low compared with the temperatures at inlet 1 and inlet 2 which were equal to 500K and 400K respectively. As a result, the first correction was to change the time-step from 0.001s to 0.01. Although the results were better than the previous, they didn't achieve the acceptable outcomes. The new time-step was applied with the three amplitudes, but in each case there was no real heat transfer; the difference in temperature between inlet 1 and

16

outlet 1 was 100K, and between inlet 2 and outlet 2 was 15K. According to this information, the time-step was increased to 0.05s.

By applying 0.05s at each amplitude for the range of frequency (0.1-1.6 Hz), high diffusion for energy was achieved. More information about the energy diffusion will be discussed in the next chapter.

CHAPRTER III

Solution Method

3.1 STAR-CCM+

STAR-CCM+ can be described as the world's most comprehensive engineering physics simulation inside a single integrated package. Many engineering problems can be solved by STAR CCM+, such as heat transfer and stress, as well as computational fluid dynamics (CFD) simulations. One of the main advantages of STAR CCM+ is that it is designed to handle large models quickly and efficiently. Using a unique client-server architecture, STAR CCM+ can accomplish meshing, solving and post-processing over multiple computing resources, but does not require any additional effort from the user [14].

STAR CCM + includes many components such as 3D-CAD modeler, CAD embedding, surface preparation tools, automatic meshing technology, physics modeling, turbulence modeling, post-processing, and CAE integration. The following sections provide a short explanation for each component.

3D-CAD Modeler

This component is a feature-based parametric solid modeler within STAR-CCM+ used to create geometry. By using this feature, STAR CCM+ can create geometry as 3D-CAD and store it as 3D-CAD models, which can then be converted to geometrical parts for integration with meshing and simulation tools. Moreover, 3D-CAD achieves a very significant goal by designing parameters to make it easy to modify the 3D-CAD models from outside of 3D-CAD. Some benefits can be obtained from 3D-CAD modeler like solving for a particular geometry, changing the size of one or more components, and quickly rerunning the case.

18

CAD Embedding

Simulations of STAR CCM+ can be imported from many sources such as SolidWorks, CATIA V5, Pro/ENGINEER, and NX. STAR-CCM+ simulations can then be set up, run and post-processed. Accurate CFD solutions are obtained more quickly and more reliably by using STAR-CCM+'s unique approach.

According to the principle of associativity, CFD results are linked directly to the CAD geometry. In addition, it's very easy to update simulation results if there are any modifications in the CAD model. This process happens by clicking the "update solution" button, allowing the rapid and thorough investigation of the design space.

Surface preparation tools

Preparing of surface is very important before running the simulations; a surface needs to be clean to apply meshing theory. STAR CCM+ has an automated process that links a powerful surface wrapper to CD-adapco's unique meshing technology. For complex geometries, meshing needs days to be completed, but the surface wrapper reduces the number of hours spent on surface to hours instead of days.

In addition, the surface wrapper provides many functions such as closing holes in the geometry and joining disconnected and overlapping surfaces, triangulating surface mesh onto any geometrical model, and providing a single manifold surface that can be used to automatically generate a computational mesh without user intervention.

Automatic Meshing Technology

STAR CCM+ has an automatic meshing option which gives a high quality mesh by generating either polyhedral or predominantly hexahedral control volumes. It also offers a

combination of speed, control, and accuracy. In addition, STAR CCM+ can automatically make conformal meshes across numerous physical domains for problems including multiple frames of reference, fluid-structure interaction, and conjugate heat transfer.

STAR CCM+ users should pay attention to the near-wall region, or extrusion-layer mesh, to generate accurate CFD simulations. By using STAR CCM+, a high-quality extrusion layer mesh on walls in the domain is it automatically produced. In addition, the user can control the position, size, growth-rate, and number of cell layers in the extrusion-layer mesh.

Physics Models

STAR-CCM+'s physics modeling capabilities include: Solvers, Time, Turbulence, Compressibility, Multiphase, Heat transfer, Combustion & Chemical Reaction, Moving Mesh, and Distributed Resistance (Porous Media).

These components have many options to make a user able to solve different cases. For example, Solver has three components: segregated, coupled, and finite volume solid stress. In this thesis, segregated solver was used to run simulations. In addition, Time includes steady state, implicit and explicit unsteady, and harmonic balance. Implicit unsteady was also used in this thesis. Finally, for Moving Mesh, only mesh morphing was used while the rest (dynamic fluid body interaction (DFBI or 6DOF), rigid body motion, and multiple reference frames (MRF)) were not suitable for this research.

Turbulence includes RANS, RSM, LES/DDES, and Laminar-turbulent transition. Compressibility includes Ideal Gas and Real Gas. Heat Transfer includes Conjugate Heat Transfer (CHT), Multiband and gray thermal surface to surface radiation, solar radiation, and discrete ordinates radiation (DOM) including participating media. Multiphase includes Lagrangian particle

20

tracking, VOF (incompressible and compressible), Cavitation & boiling, Eulerian multiphase,De-icing & De-fogging, and Melting & solidification. Combustion & Chemical Reaction includes Reaction kinetics, Eddy break up (EBU), Presumed probability density function (PPDF), Complex chemistry, Ignition, and NOx modeling. Distributed Resistance (Porous Media) includes Anisotropic, Orthotropic, User defined, and Porous baffles. These components were not used in this thesis and are mentioned here for general information about STAR CCM+.

Turbulence Modeling

STAR-CCM+ is used for inviscid and laminar flow modeling, as well as providing a comprehensive range of turbulence models such as k-epsilon (Standard, V2F, Realizable, Two-layer), k-omega (Standard, SST and BSL), Reynolds Stress (RSM – linear and quadratic), Spalart-Allmaras Turbulence models, Boundary-layer transition, Large Eddy Simulation (LES), and Detached Eddy Simulation (DES, in the new Delayed Detached Eddy Simulation or DDES formulation).

Post-processing

There are many post-processing tools in STAR CCM+ which can be used to obtain maximum value and understanding from CFD simulations. These tools can show the results as scalar and vector scenes, streamlines, scene animation, numerical reporting, data plotting, import, and export of table data, and spectral analysis of acoustical data.

CAE Integration

STAR CCM+ is used during the limited range of simulations but can be coupled with several third-party analysis packages to extend the range of possible simulations. File-base

21

coupling can be possible with Radtherm, NASTRAN and ANSYS, while Co-simulation is possible using Abaqus, GT-Power, WAVE and OLGA.

3.2 Description of the CFD Model

The apparatus consists of two chambers connected by a pipe. Each chamber is a rectangular box with an inlet and outlet. The effect of pulsating is generated at the wall of the left-hand reservoir, and it is modeled by a sinusoidal motion of the piston wall. Dimensions and some properties are provided in figure 3.
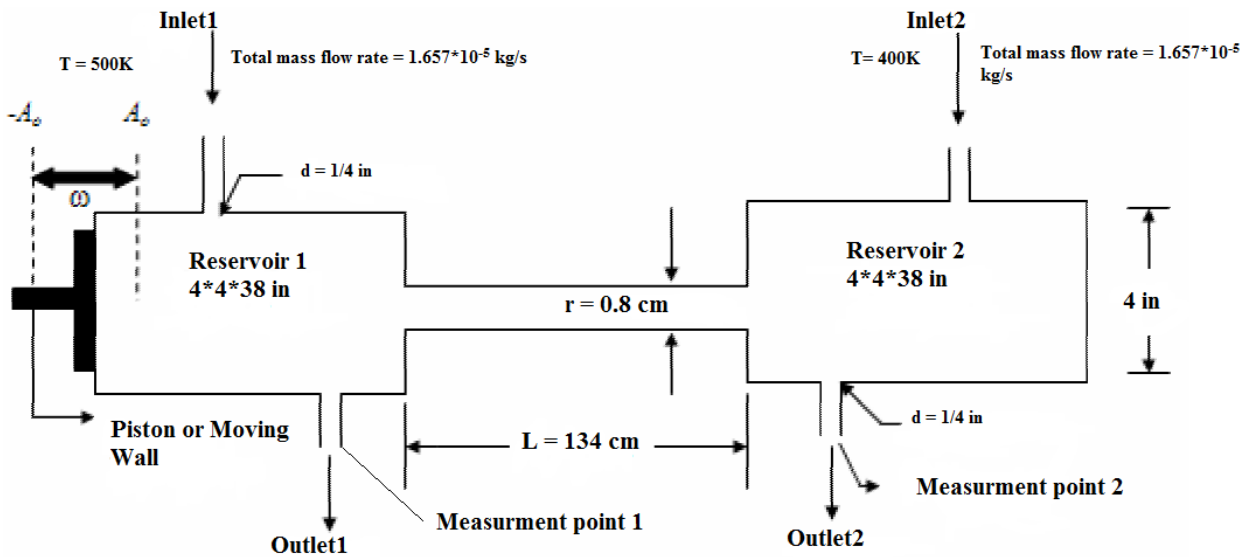

Figure 3: Sketch of a 2D section of the device used in the CFD Simulation.

To achieve diffusion of fluid, the moving cylinder is substituted by a moving wall in one of the extremes as it is shown in figure 3. The model requires creating the volume that simulates the original device as closely as possible, which is one of the biggest challenges of this study.

3.3 CFD Grid Generation

The model volume was meshed in a multi-block unstructured hexahedral grid with a number of 1039321 cells, 6241463 interior faces, and 5059778 vertices. The mesh was clustered near the sidewalls to accommodate the accurate modeling of the boundary layers, see figures.
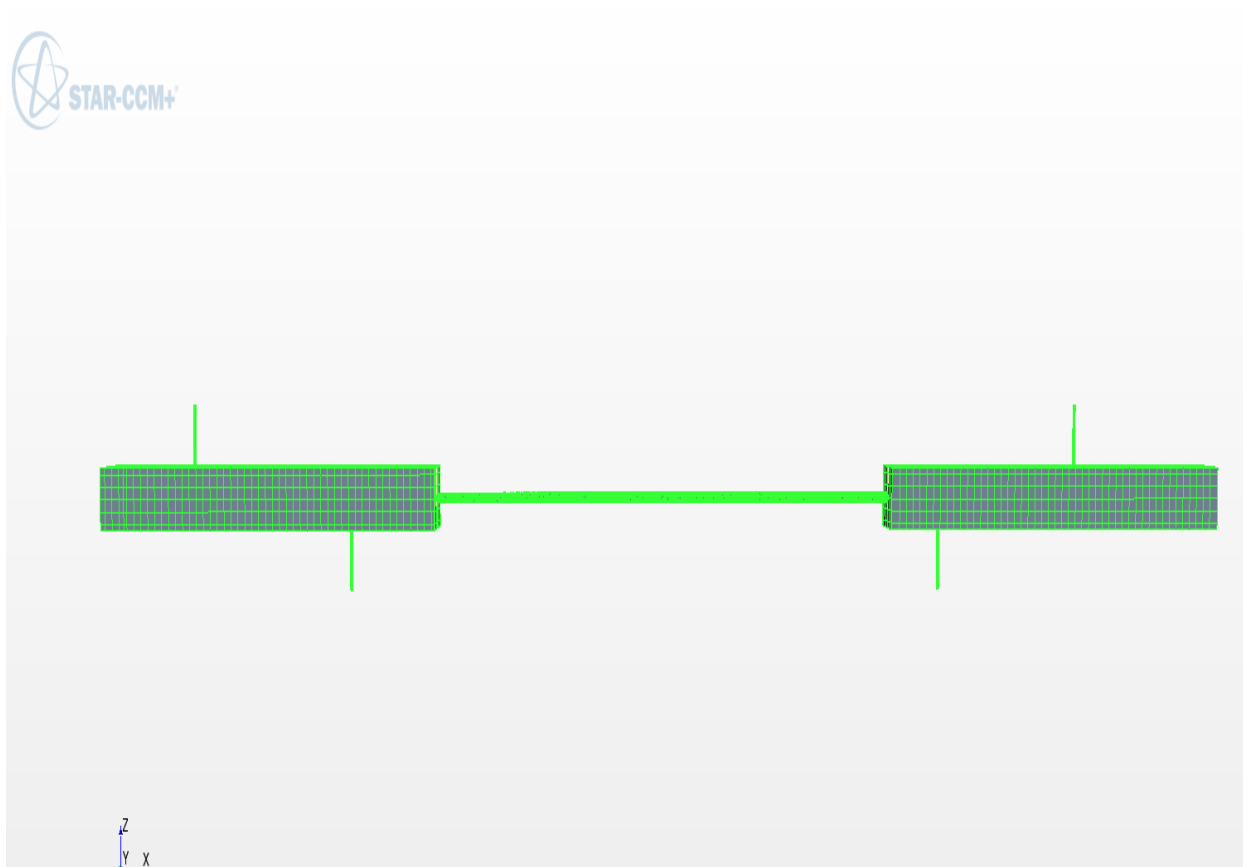

Figure 4: Sketch of a 2D section of the device used in the CFD Simulation
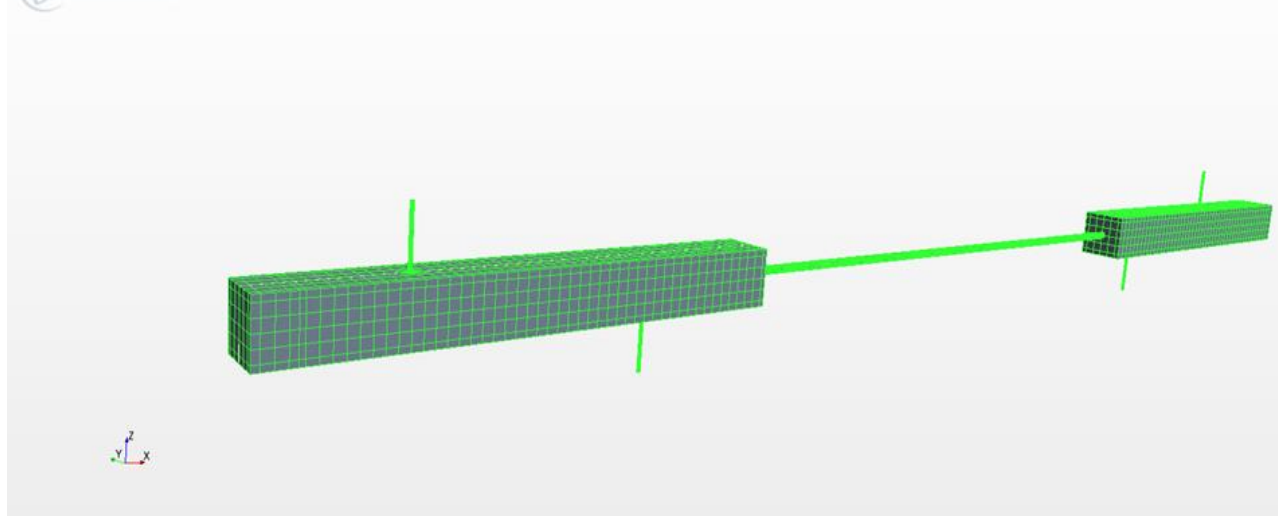
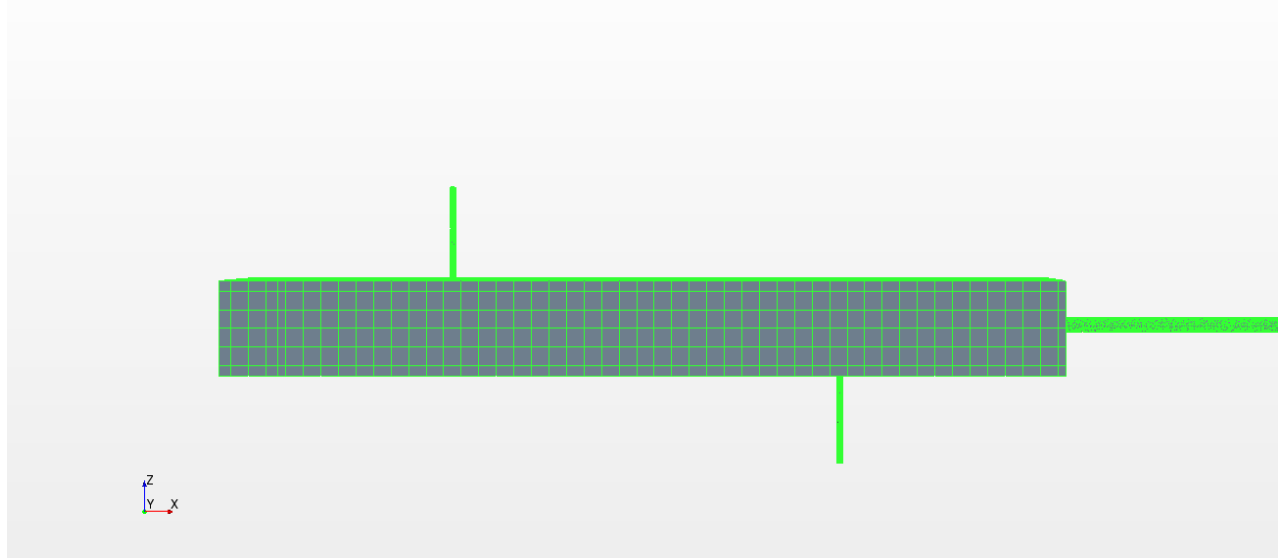*Figure 5: 3D section of the device used in the CFD Simulation*

Figure 6: Sketch of a 2D section of the left hand of the device used in the CFD Simulation
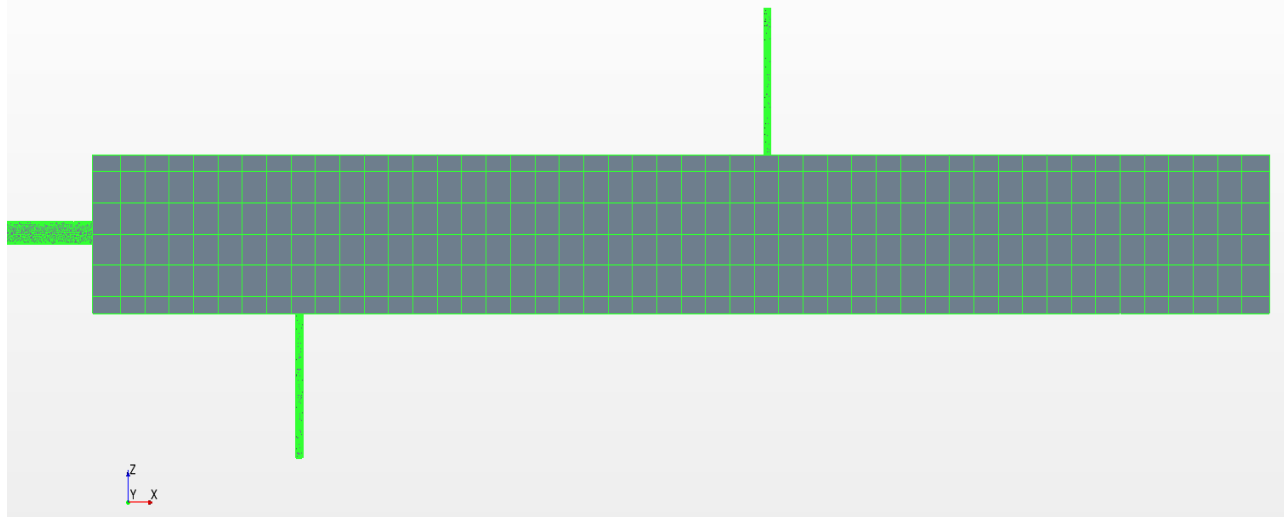
Figure 7: Sketch of a 2D section of the right hand device used in the CFD Simulation

3.4 Computational Fluid Dynamics solver

Discretizing the surface and spaces around the boundaries of computational domain to be utilized when the fluid flow problems are numerically solved. There are three modules for CFD software: the pre-processor, the solver and the post-processor [15].

Pre-processor: In this module, all variables and fluid properties must be setup to define the problems such as pressure and velocity.

Solver: Solver provides an important function to STAR CCM+ by computing the solution of CFD problem and solving the governing equations. To obtain an accurate solution of the partial differential equations, convergence should be achieved.

Finally, post-processor is used to process and visualize the results obtained from the solver.

3.4.1 Preprocessing

All preprocessing is performed using STAR-CCM+. Preparing geometry, defining the simulation, generating the mesh, preparing for analysis, running the analysis and analyzing the results is the general workflow in this software. In this thesis, only the most relevant information for the two cases is discussed.

3.4.1.1 Unstructured meshing in STAR-CCM+

An unstructured mesh has been applied for all the simulations in this thesis. In STAR-CCM+ this is available by using the parts-based meshing for CAD geometries. Parts-based meshing detaches the meshing from the physics and provides a flexible and repeatable meshing pipeline. This strategy provides several advantages over region-based meshing. The mesh created will be hexahedral.

For the surface mesher, the surface "remesher" is used to re-triangulate a closed starting surface to obtain a high-quality surface mesh. Usually, when improving the quality of imported tessellated geometry is needed, the surface mesher is used. This has been done because the geometry was imported directly and there were some holes and edges. By using surface "remeshing" with surface repair tools, such as hole-filling and edge-zipping, it became easy to get a closed surface. Many of these repair tools can be automated by using the automatic surface repair tool to minimize the manual effort required [14].

On the other hand, in STAR-CCM+, there are different types of meshing models that can be used to generate a volume mesh starting from a suitably prepared surface mesh. For this thesis, the trimmed mesher has been applied. Hexahedral cells can be generated by using the trimmer meshing model that uses a template mesh that contains refinement that is based on preparing the

local surface mesh size and local refinement controls. The transitioning of the mesh cell sizes from small to large are controlled by Growth parameters at the surface and far field. The cell size bounds at up or bottom can be controlled by maximum or minimum or both cell size. Moreover, the template can be aligned in any direction in a user specified Cartesian coordinate system.

In addition, the trimmer meshing provides the ability to refine cells in a wake region, represents the volume of fluid at the rear of a moving body, in modeling external aerodynamic flows.
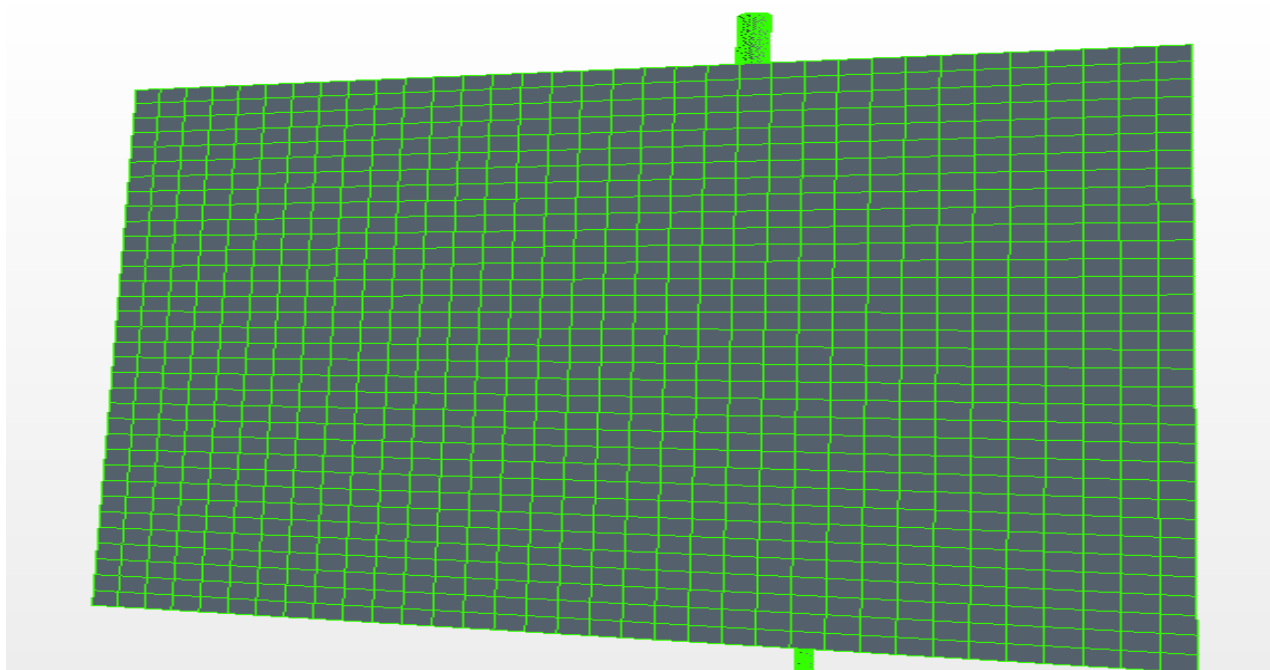
Figure 8: Trimmed mesher

3.4.1.2 Mesh diagnostics

A full mesh diagnostics report was ran for all meshes generated in this thesis in order to check whether the mesh was good. There were many factors that the mesh diagnostics report applied such as:

- Mesh validity

- Face validity

- Volume change statists

- Maximum interior skewness angle

To ensure the mesh validity, unclosed cells, invalid cells or vertex references, zero face area, and zero or negative volume cells are checked. The face validity is an area-weighted measure of the correctness of the face normal relative to their attached cell centroid while the volume change statistics describes the maximum and minimum ration of the volume of a cell to that of its largest neighbors. A skewness angle of 90 degrees or more, which can occur in concave cells, are problematic in STAR-CCM+. Due to this, it is not recommended to have any skewness angle greater than 85 degrees. For all analyses the maximum skewness angle was kept below 50 degrees.

For different meshes, the aspect ratio was also investigated. The cells in the mesh are preferred to be regular polygonal cells, not highly stretched. This can be investigated by using a scalar scene and the cell aspect ratio field function. In addition, the bad cell indicator field function was applied in all meshes to check for cells that are considered bad.

3.4.1.3 Applied boundary conditions

To apply boundary conditions in the computational domain, they must be given physical properties. Below, some types of boundaries were used in STAR CCM+ in this thesis.

- **Velocity Inlet:** Velocity inlet is specified in STAR-CCM+ directly. The boundary face pressure is extrapolated from the adjacent cell using reconstruction gradients.

- **Pressure Outlet:** Pressure Outlet specifies the pressure on the outlet boundary to be equal to zero. At the pressure outlet the boundary face velocity is extrapolated from the interior using reconstruction gradients.

- **Wall:** By using this boundary condition, the tangential velocity at the boundary is set to zero. The boundary layer face pressure is extrapolated from the adjacent cells using reconstruction gradients. There will not be any velocities through a boundary defined as a wall.

3.4.1.4 Applied physical models in STAR-CCM+

A physical phenomenon can be defined by the physic module that is presented in STAR-CCM+. The purpose behind using the physics modules to define the primary variables of the simulation (in this case pressure and velocity) and the mathematical formulation used to find the solution. A combination of models is necessary for the complete definition of a physics continuum.

In STAR-CCM+ the physics models and methods are selected using a physics continuum. In all analyses in this thesis, the following physics models have been used:

- Space: Three Dimensional

- Time: Implicit Unsteady

- Material: Gas

29

-   Flow: Segregated Flow

-   Equation of State: Constant Density

-   Viscous Regime: Laminar

3.4.2 Solver

The implicit unsteady solver is the only available time solver for constant-density transient analysis in STAR-CCM+, and has thus been applied. A 2nd order temporal discretization scheme has been applied. For flow model, there are two types of flow. Coupled and segregated flow. The segregated solver is faster and uses less memory for incompressible flow according to Steve - adapco; Support, Star-CCM+. The segregated flow model solves the flow equations (one for each velocity component and one for pressure) in an uncoupled manner.

3.4.3 Post processing

Various kinds of plots and scenes can be created by STAR-CCM. Before running the simulation, the plots and scenes are set up, and can be analyzed when the stopping criteria is satisfied and the simulation is finished. The plots and scenes can be viewed while the simulation is running, which is initially informative. In this thesis, the plots and scenes have been used also to evaluate when the flow is considered to be fully developed. Reports, monitors, plots, graphic scenes and animations were created in STAR-CCM+.

In this thesis the following scenes have been used to obtain the graphical results:

-   Vector scene for velocity

-   Scalar scene for temperature

-   Scalar scene for the pressure

3.4.3.1 Running simulations

In STAR-CCM, the simulations can be run to give stopping criteria. The simulation is saved, and changes can be made in the simulation before running a new simulation.

Some changes tested during running the unsteady state in this thesis are:

- Changing the time step before running the simulation or after the solution is obtained to rerun new one.

- Changing number of iterations per time step to get the right number that gives the suitable solution.

- Changing boundary conditions, e.g velocity at the inlet boundary

- Generating a new mesh

- Changing the frequency for saving the solution to the history file and also changing the solution history file

Note: it is not possible to change the computational domain. Other than this, many variables may be changed in STAR-CCM+ and this is very useful.

3.5 Fluid flow and Energy Interaction

The diffusion of energy is one of the familiar phenomena in nature. For example, if two gasses with different temperatures in two tanks connected by a tube are mixed, the movement of the hot gas will be toward the cold gas till equilibrium is achieved [9]. It's a simple example of what will be discussed in this thesis.

Figure 9 shows the mechanism of diffusion of energy in a long cylindrical pipe between two large reservoirs.

31
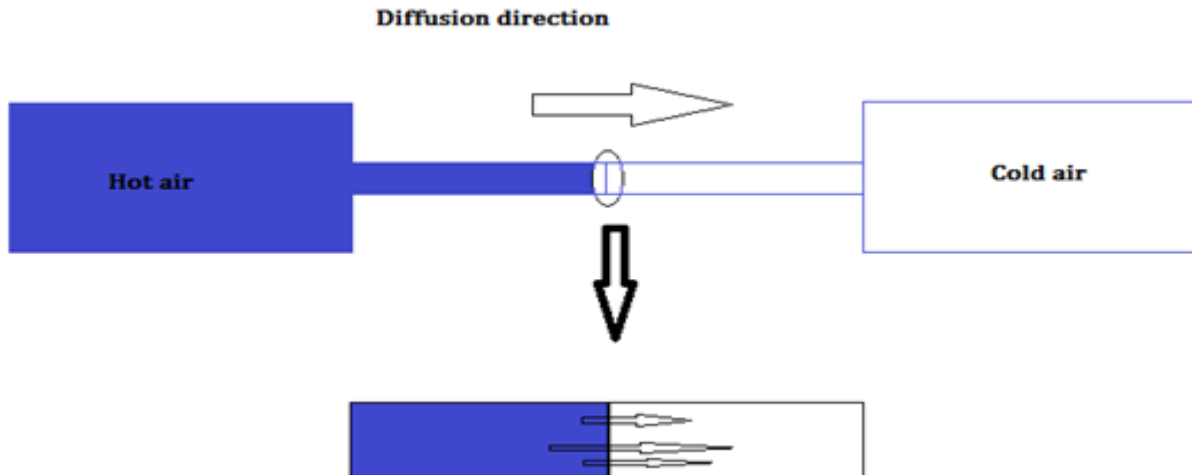
Figure 9: Diffusion of energy

From the figure above, it can be seen that the diffusion accrued in only one direction: toward the right reservoir along the x-axis. Moreover, the diffusion gradient was straight during the whole steady process due to the absence of convection

However, the steady state can be explained clearly by governing equations. For the conservation of mass, the loss in mass is zero for incompressible flow

$$\nabla . \vec{V} = 0 \text{ (continuity)} \tag{31}$$

The equation of energy appears without convection enhanced velocity as shown below.

$$\rho_c \frac{\partial T}{\partial t} = k \nabla^2 T \tag{32}$$

From the equation above, the absence of convection seems clear and it means the heat transfer occurs only by conduction.

On the other hand, in unsteady state situations, the mechanism of diffusion has been used to create curves to calculate heat transfer at diverse tidal displacements and frequencies. The description of the functionality of this oscillatory device is explained based on the convective flow motion for two air flows: hot and cold flows (figures10 and 11).

32
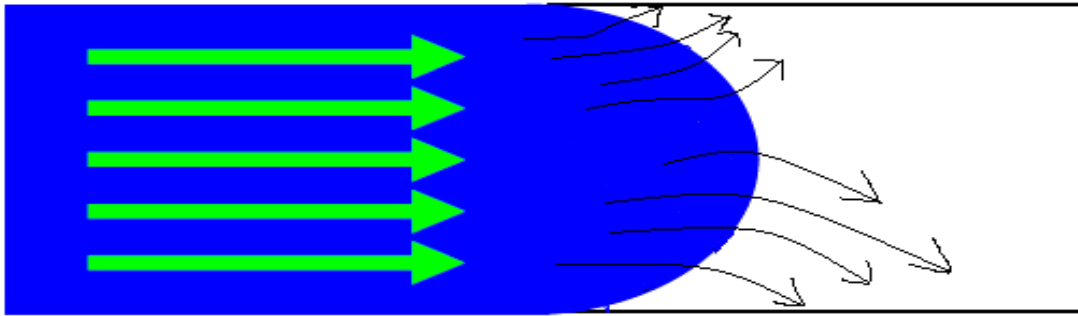
Figure 10: First half of the cycle

In the first half of the oscillation cycle, figure 10, a hydrodynamic boundary layer forms and causes radial diffusion gradients generating a movement of the fluid contained in the hot air from the core to the wall.

The hot air moves fast by forced convection in different directions far away from the centerline where the maximum velocity is attained above and below the core during the transfer to the cold side. Heat transfer by conduction keeps straight in the same direction.

In the second half of the oscillation cycle, figure 11, the hydrodynamic boundary layer forms in reverse and again causes radial diffusion gradients forcing the diffused fluid to migrate from the wall to the core.

Figure 11: Second half of the cycle

At the start of the first half of the next oscillation cycle, figure 12, the hot air in the fast moving core of the tube is transferred by convection down the tube core and again diffuses towards the wall due to high diffusion gradients.
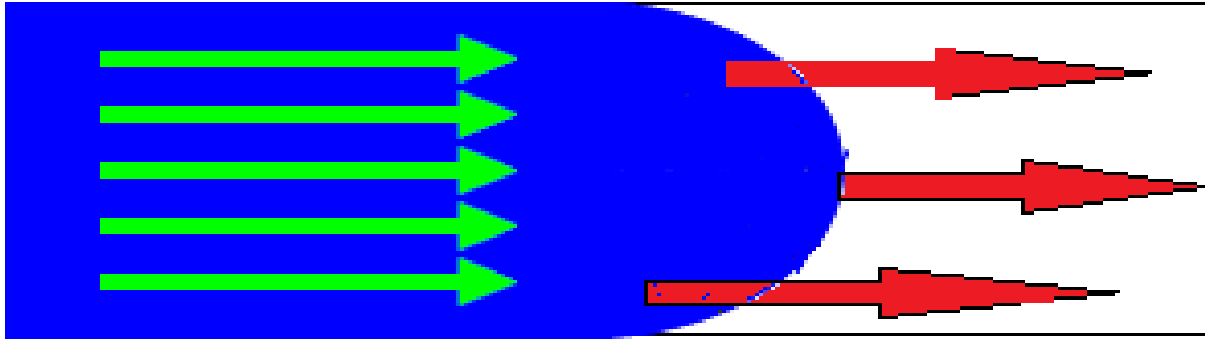
Figure 12: First half of the next cycle

Wall – no slip and zero velocity

Core – maximum velocity
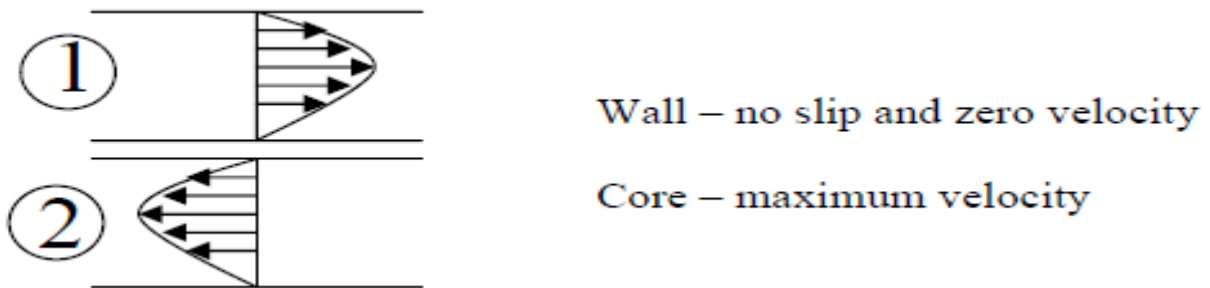
Figure 13: One cycle for fluid (air)

The Navier-Stokes equations in the unsteady state situation are more effective because of the use of external force (piston) and the enhanced convection is applied to increase the heat transfer from the model. Forcing the fluid by a moving piston improves the results and gives the governing equations in the formulas below.

$$\nabla \cdot \vec{V} = 0 \qquad\qquad \text{(Conservation of mass)} \qquad (33)$$

$$\rho \, \frac{\partial \vec{V}}{\partial t} + \rho_c \, (\vec{V} \cdot \nabla) \, \vec{V} = -\nabla p + \mu \, \nabla^2 \, \vec{V} + \rho \, \vec{f} \qquad \text{(Conservation of Momentum)} \quad (34)$$

$$\rho_c \, \frac{\partial T}{\partial t} + \rho_c \, (\vec{V} \cdot \nabla) \, T = k\nabla^2 \, T \qquad\qquad \text{(Conservation of energy)} \qquad (35)$$

From the equations above, the oscillatory flow provides enhanced convection to the CFD model by adding velocity to the equation. Moreover, a moving piston adds enhanced conduction $(k\nabla^2 T)$ and enhanced convection $((\rho_c (\vec{V} \cdot \nabla) T)$ to energy equation (28).

3.6 Implementation (Initial Solution without the Oscillatory Wall)

The goal of this thesis was to get the results from STAR CCM+ without using the moving wall and to make the CFD model ready to receive the effect of the oscillating motion after a steady state is reached because of pure diffusion.

The governing equations are solved for air in the CFD model. The mass flow rate of hot air at inlet 1 is equal to the mass flow rate of cold air at inlet 2. The air parameters at both inlets were set up so STAR CCM+ would recognize the fluid to minimize numerical error.

In this case, the diffusion of energy by conduction only was considered without using any external force to generate convection. However, the diffusion of hot air was more than that of cold air which was predicted due to the principle of natural conduction that says heat transfer moves from a hot region to a cold region until equilibrium is achieved, as shown in the figures above. According to the explanation in the previous section, the center of the cylinder, as well as the outlets, were the measurement points that were chosen to calculate the. The results were exported from STAR CCM+ to EXCEL and then compared to what was expected. The figure below shows the diffusion of the air.
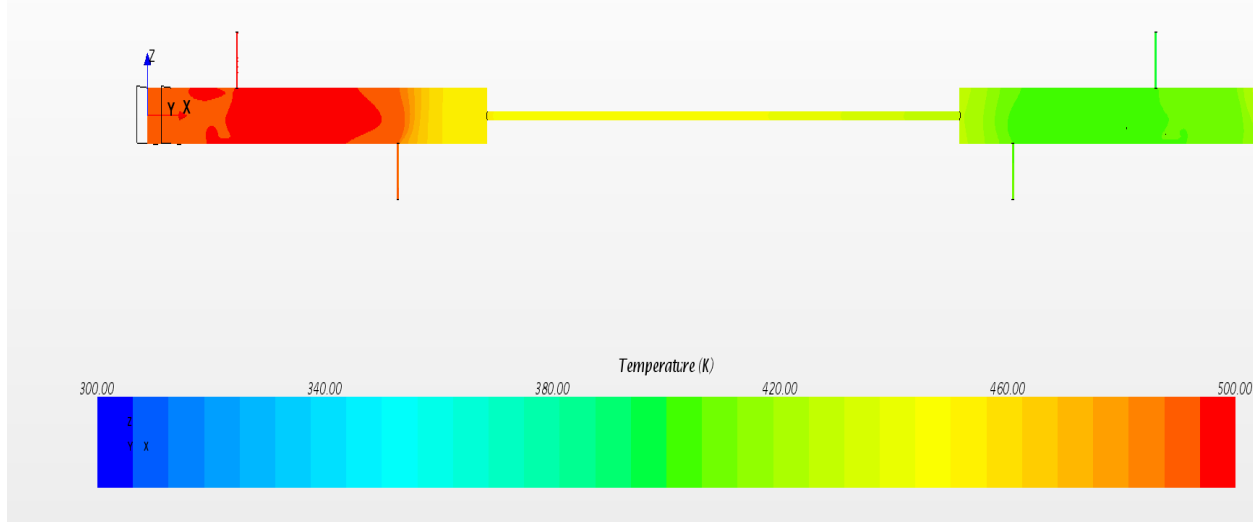
Figure 14: diffusion of are before Oscillation of the Left Wall

In summary, this case was used to prepare the CFD model for the unsteady state. The simulation was run until the convergence was achieved. The temperatures at outlet 1 and outlet 2 were 490K and 410K respectively. These results were the same for unsteady state without motion.

3.7 Oscillatory Piston Model for CFD Formulation

There are two approaches in STAR CCM+ to set the motion of the wall in terms of a sinusoidal position. The first one is a moving wall and the Dynamic Overset Behavior. In this thesis only the moving wall was used to get the expected results.

3.7.1 Moving wall implementation

The moving wall was the best approach for the model used in this thesis. The morphing was used to define the equation of motion at the left-hand wall as shown below.

$$V = A*\omega*\cos(\omega t) \tag{35}$$

For example, for one simulation, the equation is:

$$0.067*2*3.1415*0.2*\cos(2*3.1415*0.2*\$Time)$$

Where

$$A = 5\% \ L= 5\% \ *1.34 \ m = 0.067 \ in$$

$$\omega = 2\pi$$
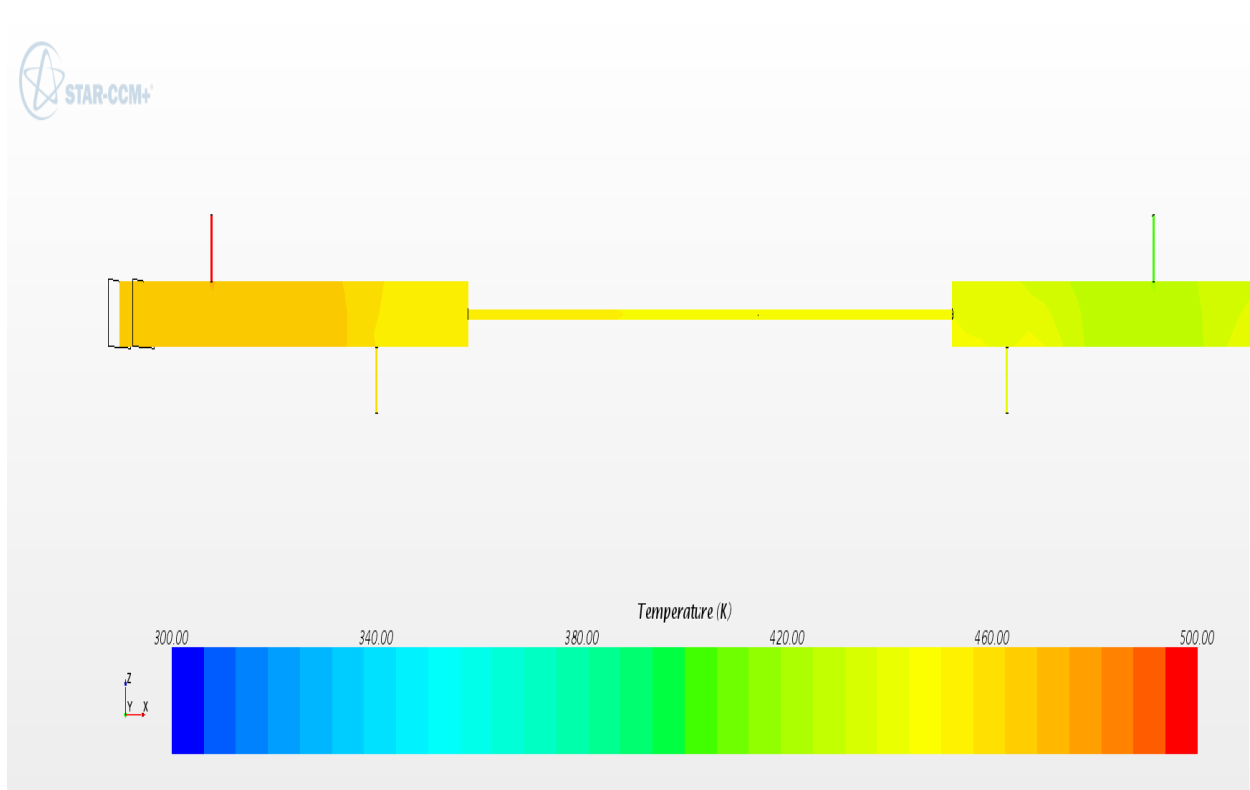
Figure 15: diffusion of are after Oscillation of the Left Wall

In this section, the mesh morphing procedure in Star-CCM+ is explained. The volume mesh in a simulation is the mathematical description of the geometry of the problem being solved and it is formed by vertices, faces and cells. The morphing is the type of motion which makes possible the deformation of the computational mesh in response to various causes. During the process of

morphing, the mesh vertices are redistributed in response to the movement of a set of control points.

The boundary conditions at the left hand wall were set after the morphing code was written. There were two options to set the motion of the piston: morphing and translation. According to Steve-adapco support, morphing is good with a moving wall while translation is suitable with an overset mesh. Since the moving wall functioned perfectly as expected in STAR CCM+, this proved to be successful. As a result, the results showed the diffusion of energy moving from the hot reservoir on the left to the right with high amounts of heat transfer. The method proved to be accurate because the fluid behaved as expected. The motion reflected the system behavior because it was oscillatory. In addition, the grid deformed with the fluid to obtain an oscillatory motion of both the fluid and grid.

The description of the motion must be specified on the vertices. Due to the pulsatile nature of the wall motion, it is important that the vertices' positions of the moving wall are returned to their original positions at the end of the cycle. It is very important to establish the original positions of the mesh at the end of each cycle, otherwise the mesh can be gradually deformed with time and lead into negative mesh volumes which could abruptly stop the simulations. In the following figures, the movement of the piston is shown.
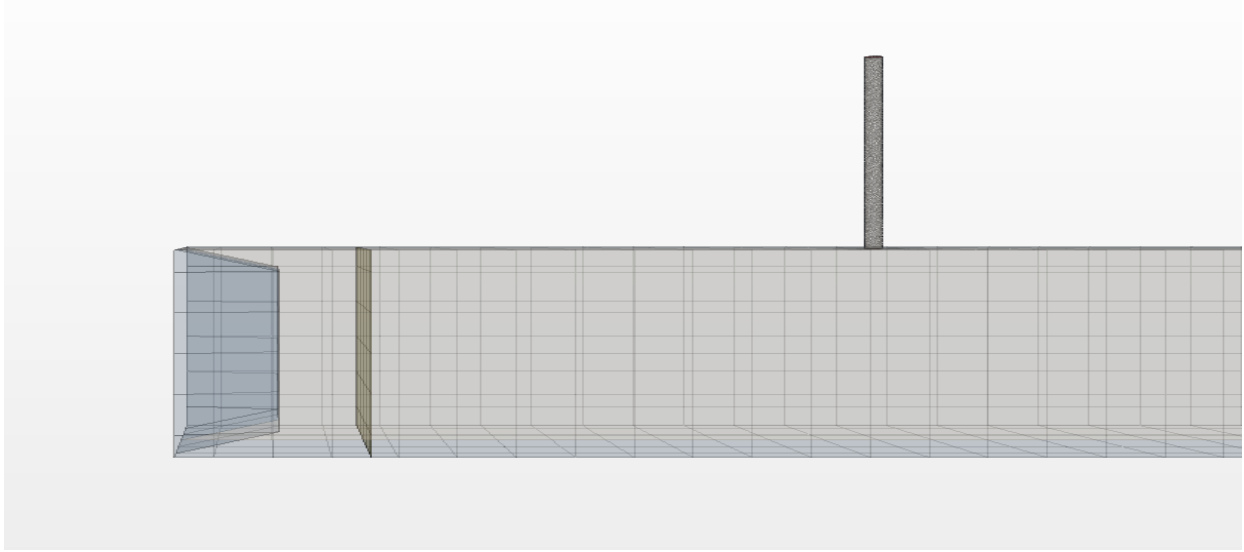
Figure 16: moving wall in the first half of the cycle.
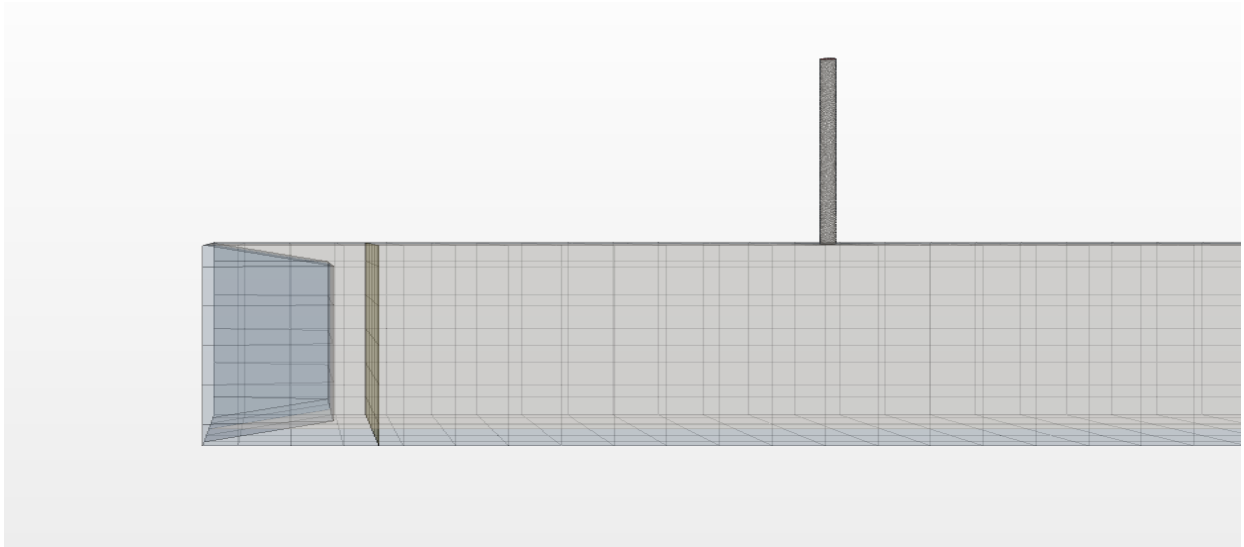
Figure 17: moving wall in the first half of the cycle.
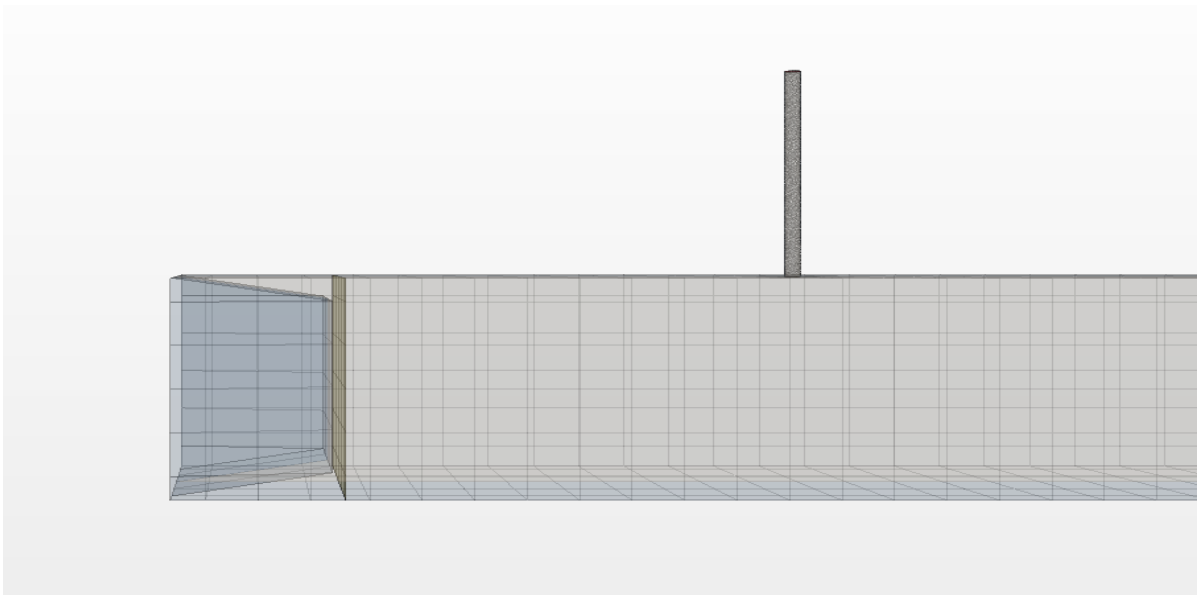
Figure 18: moving wall in the first half of the cycle
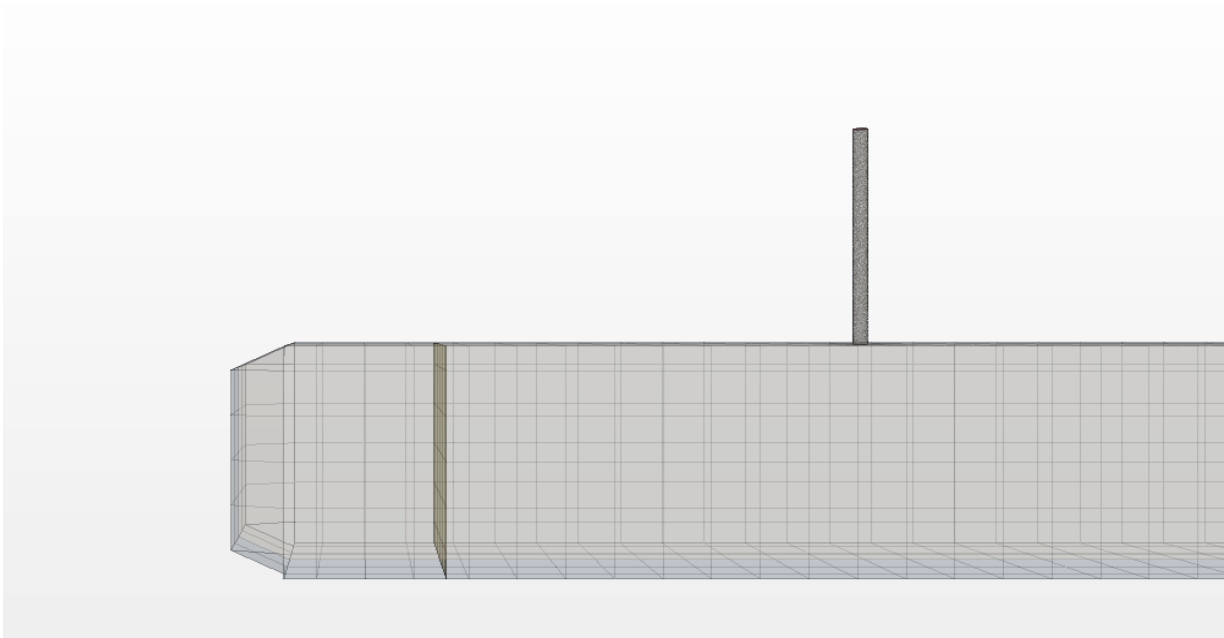
Figure 19: moving wall in the second half of the cycle
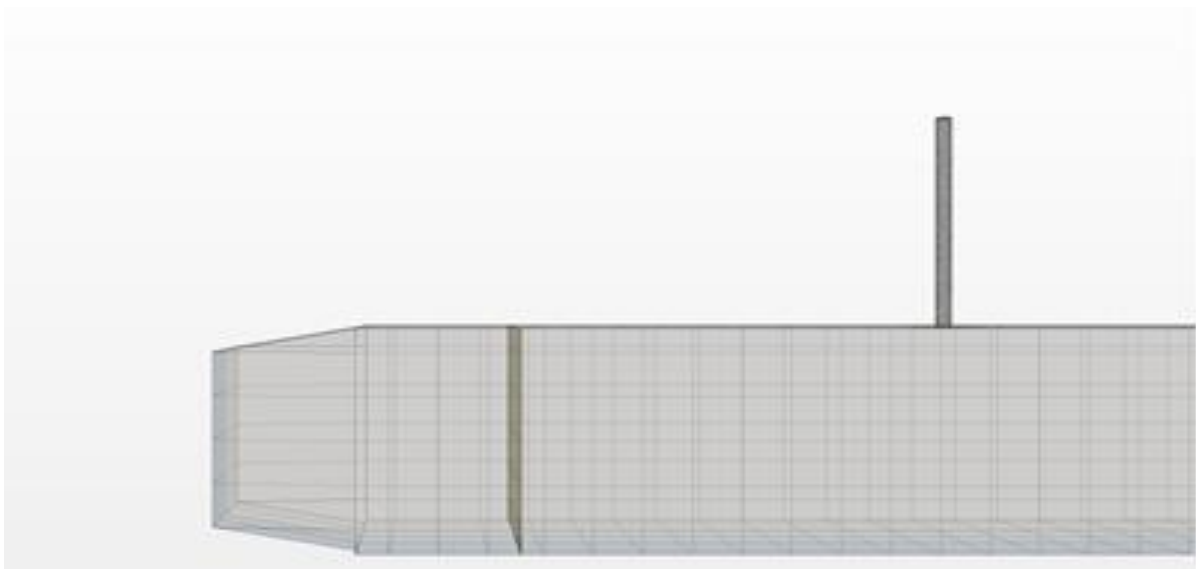
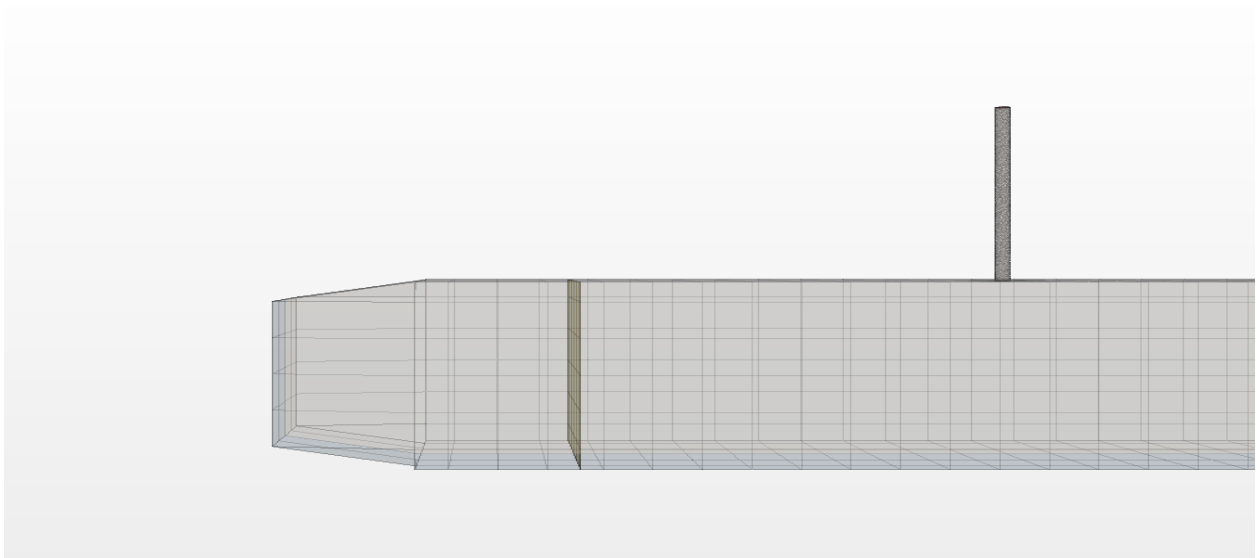Figure 20: moving wall in the second half of the cycle.

Figure 21: moving wall in the second half of the cycle

CHAPTER IV

Results and Discussions

The initial consideration was that the diffusion in the left side was going to transfer with high heat transfer to the right side due to the motion of the piston. Furthermore, the temperature at outlet 1 was expected to decrease while the temperature at outlet 2 was increasing at higher frequency values and amplitudes.

In order to assess the validation of the CFD model, the results were expected to be within the range between 500K-400K and they achieved the goal perfectly. To evaluate and analyze results from STAR CCM+, different amplitudes were considered: 5%, 7%, and 10% tidal displacement to tube length ratios. The corresponding range of frequencies was set from $0.1 - 1.6$ Hz for each amplitude ratio. Many plots for temperature and heat transfer were chosen to explain the process. In this section, there are two results that will be discussed. The first is the values of temperatures at the outlets, and the second is the values of heat transfer from the entire model.

4.1 Decreasing and increasing Temperature

The difference between temperatures at outlet 1 and outlet 2 was the important thing that was considered in this thesis and the main goal. The temperature was changed due to changing the frequency and amplitudes. However, the decrease in the temperature at the outlet in the left side was clear. For example, at frequency 0.1 Hz and amplitude 5%L, the temperature was 454.526K while the temperature at outlet 2 was 445.284K. These results were expected due to the small frequency. Moreover, by increasing frequency, the temperature at the left side decreased as shown in the following figure.
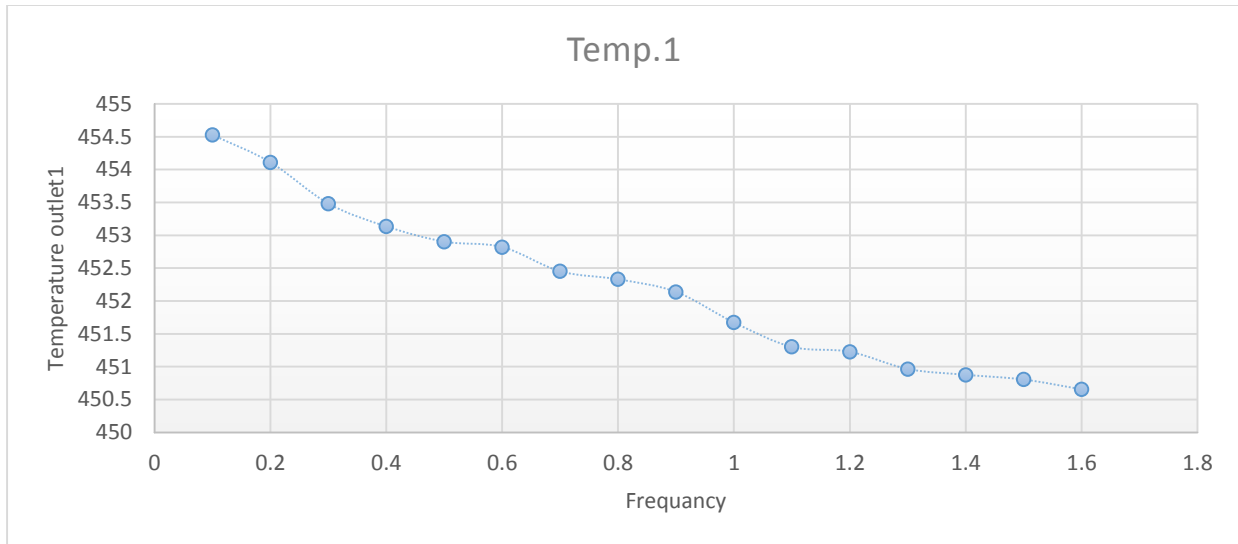
Figure 22: decreasing the temperature at outlet 1 at 5%L

From figure 22, the effect of the movement of the piston is playing a vital role to improve the enhanced convection in the model. For instance, the enhanced convection becomes more active and transfers to the right side of the model when the velocity of the piston increases by increasing the frequency. As a result, the temperature at outlet 1 decreases. The following figure shows the difference between the graphs of temperatures at the outlets.
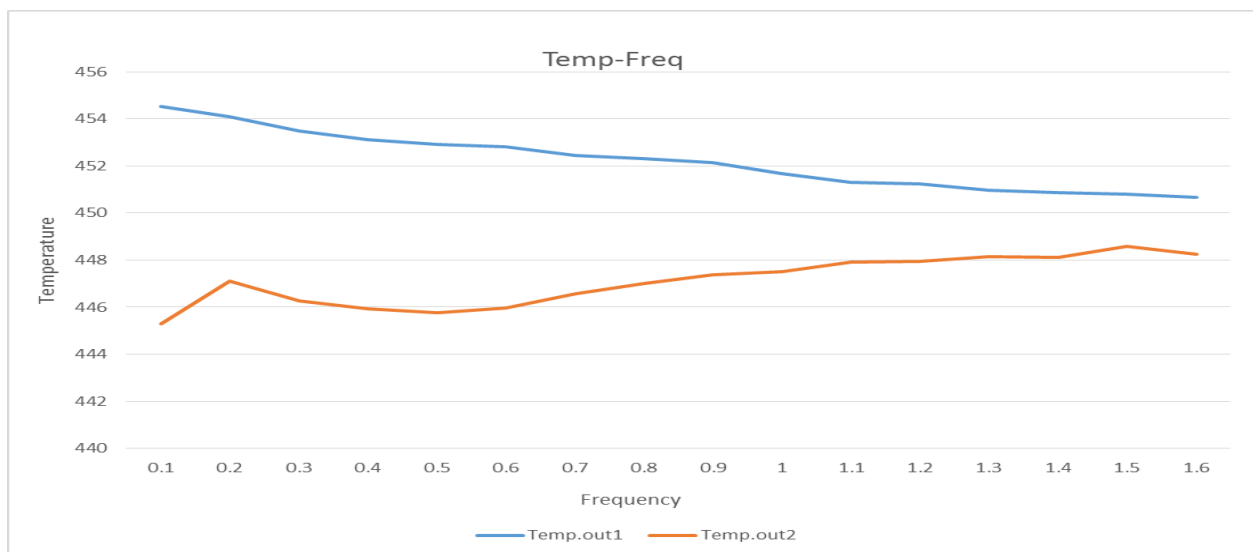

Figure 23: outlet 1 and outlet 2 temperatures at 5%L

43

The situation was similar with case 2 and case 3 with amplitudes 7% and 10%L, but there was little difference with the temperatures as shown below.
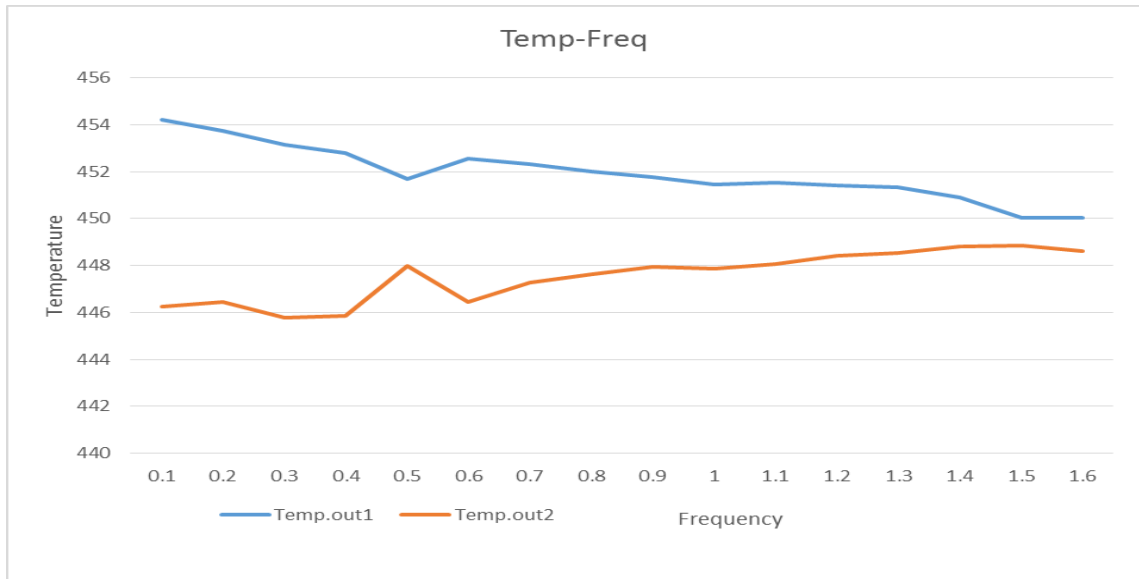
Figure 24: Temperatures at outlet 1 and outlet 2 at 7%L
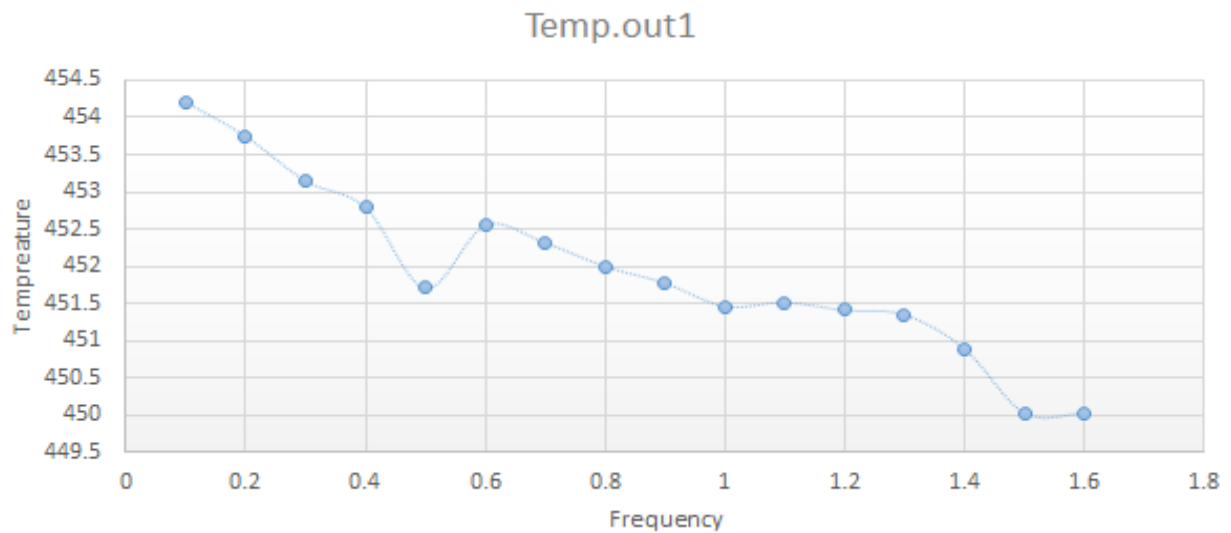
Figure 25: decreasing the temperature at outlet 1 at 7%l

44
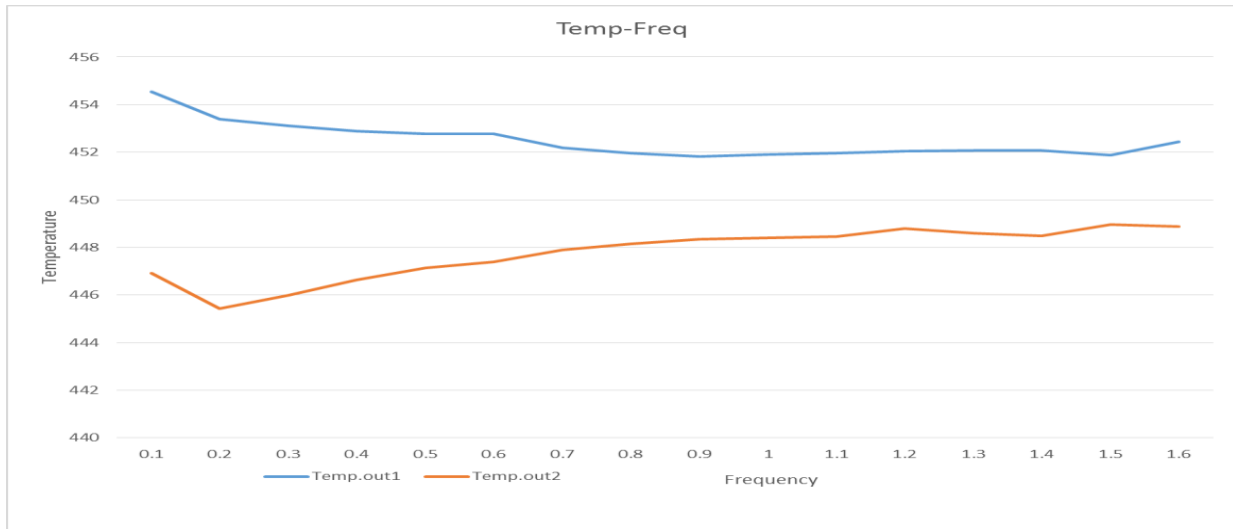
Figure 26: Temperatures at outlet 1 and outlet 2 at 10% L
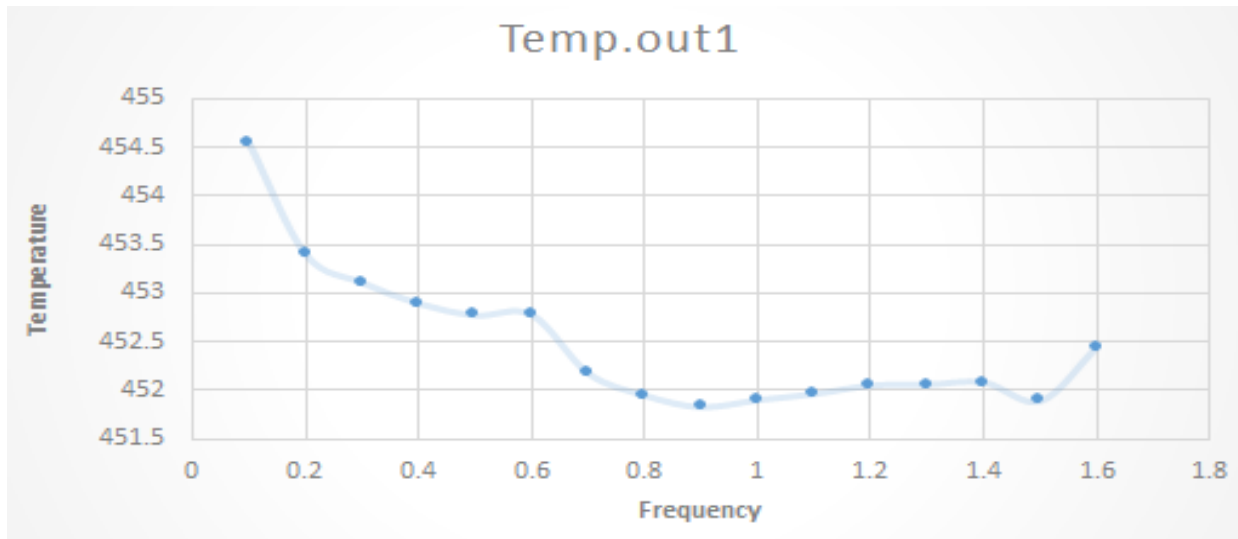
Figure 27: decreasing the temperature at outlet 1at 10% L

From the results, there is an important note: because of the moving of the piston forward and backward, there is an expected decrease or increase of the temperature. For example, for case 4 with 5%L amplitude, the temperature at outlet 1 was 452.788K and for case 5 was 451.707K. This was expected because of a high frequency at case 5, and that increased the velocity of the

45

piston. As result, the temperature was decreased. On the other hand, the temperature at case 6 was unexpected because it was more than the temperature at case 5. This happened because the simulation was done while the motion of the piston was to the left side (backward) as shown.

Table 1: The difference in temperature

7%L	v=1.7m/s	
Case#	Frequency (Hz)	Temperature (K)
Case4	0.4	452.788
Case5	0.5	451.707
Case6	0.6	452.459

4.2 Increase of heat transfer

This thesis is considered successful because it achieved the main aim that was studied for more than a year. The results of heat transfer from the model were very good and they showed a big difference between the heat transfer in the steady state and unsteady state. In addition, the amount of heat that transferred from the whole body increased by increasing the frequency and amplitudes in the unsteady state. From the figure below, the increase of the power was noticed from the values of frequency 0.1-1.4 Hz, then went up again at the last value.
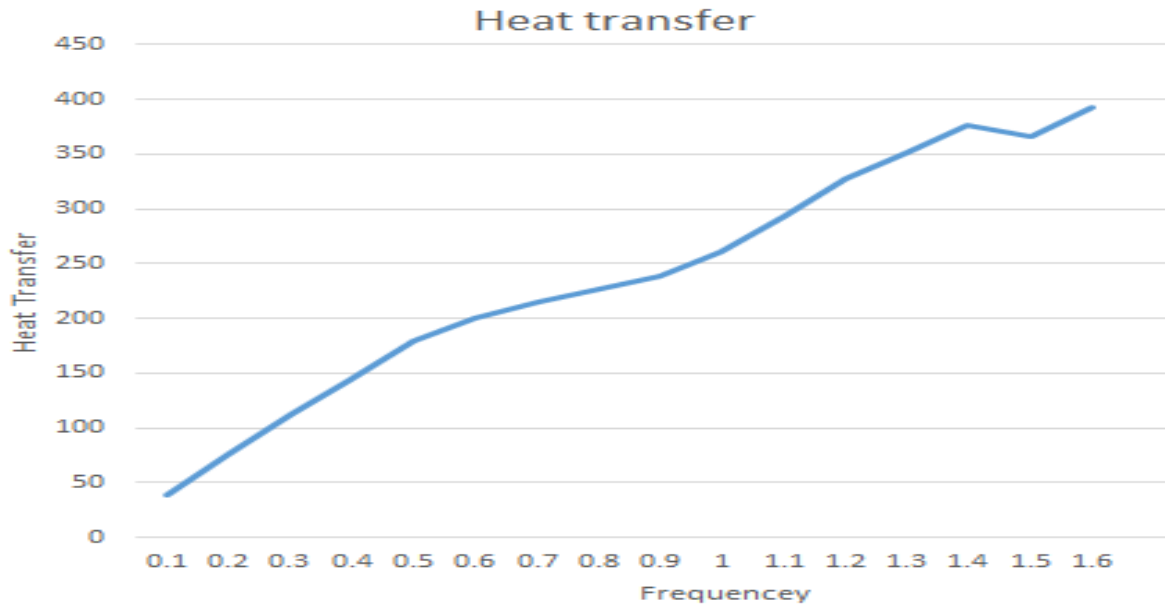
Figure 28: Heat transfer at 5%L
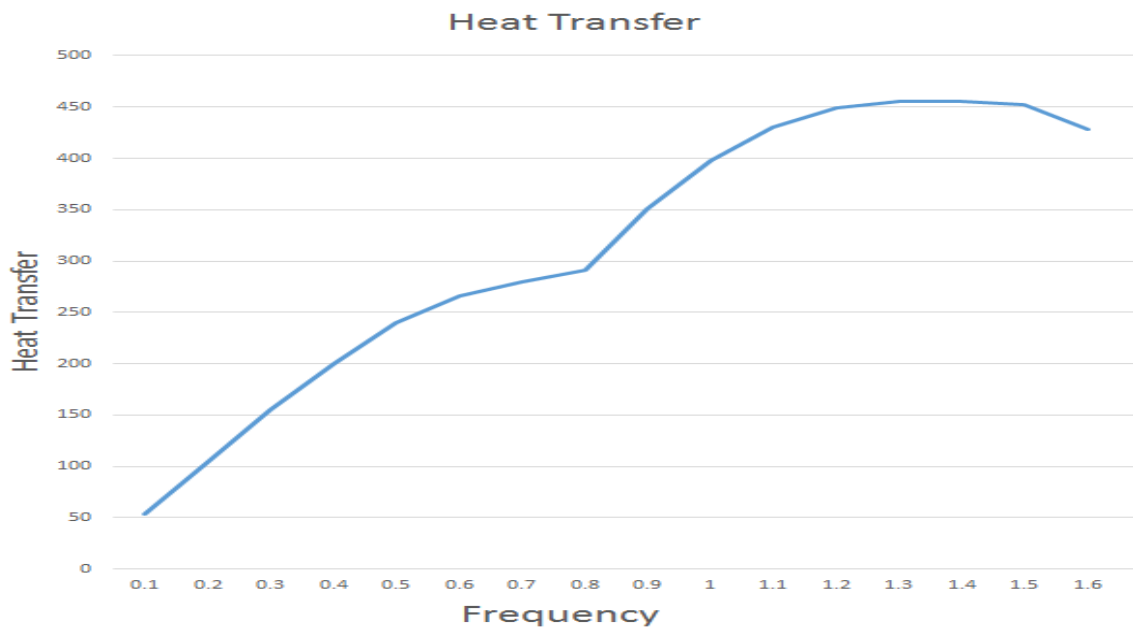
Figure 29: Heat transfer at 7%L

47
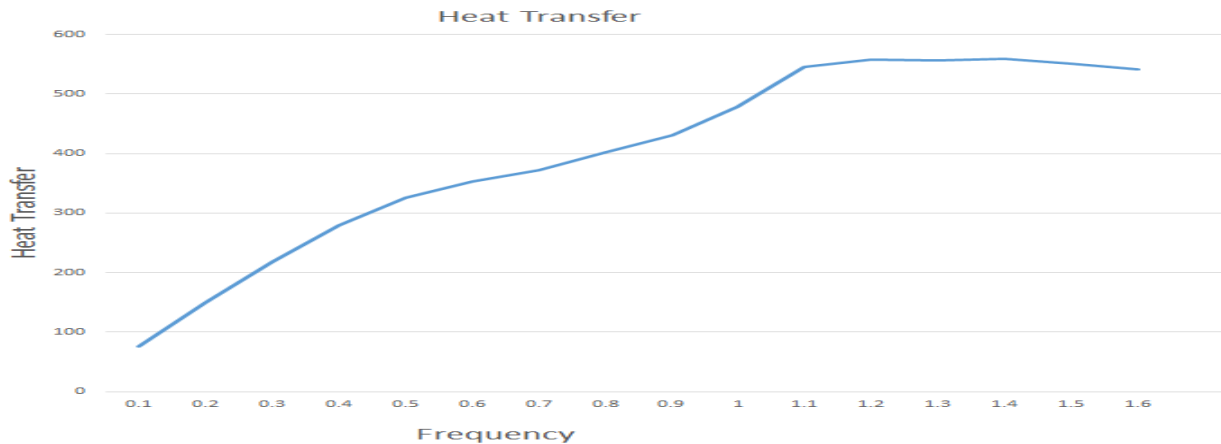
Figure 30: Heat transfer at 10%L

From the figures above, the diffusion of energy occurred from the left-hand to the right-hand crossing the duct. The oscillatory flow improved the enhanced convection many times and transferred high amounts of the energy with very good results. These results will give more motivation to do more research about enhanced heat transfer at Embry Riddle aeronautical University in the future.

The following tables explain the difference of the heat transfer before and after using Oscillatory flow.

Table 2: Heat transfer before Oscillation of the Left Wall

Regime	Heat Transfer(W)
Steady State	1.348

Table 3: Heat transfer after Oscillation of the Left Wall

Case# (AVERAGE)	Heat Transfer (W)
Case 5%L	137.5
Case 7%L	313.24
Case 10%L	400

CHAPTER FIVE

Conclusion

A three-dimensional time-accurate CFD model has been developed to simulate an oscillating-wall heat exchanger. The model consists of two chambers with inlets at two different temperatures, an oscillating piston wall on one of the chambers, and a connecting tube. Several cases are carried out reporting on heat transfer enhancement as a function of frequency and tidal displacement to connecting tube diameter.

Simulations were performed to analyze the effect of oscillations on the heat transfer. A simulation was first carried out in steady-state to serve as the baseline for comparison with time-accurate oscillating results. The remaining simulations consist of altering the frequency and tidal displacement of the moving wall to analyze their effect on the heat transfer between the two chambers. The results suggest that the heat transfer is enhanced as a function of the frequency and tidal displacement of the moving wall and that there should be an optimal point. Results are presented in the form of contour and vector plots of the temperature and velocity fields as well as plots of the heat exchanger outlet temperatures as a function of frequency and displacement.

Results of this study will be useful as a guide for the design and miniaturization of an oscillating device for enhanced heat transfer in further research projects.

References

1. Kurzweg, U. H., and Zhao, L. D., 1984, "Heat Transfer by High Frequency Oscillations: A New Hydrodynamic Technique for Achieving Large Effective Thermal Conductivities," Phys. Fluids, 27, pp. 2624–2627.

2. Kurzweg, U. H., 1985, "Enhanced Heat Conduction in Fluids Subjected to Sinusoidal Oscillations," J. Heat Transfer, 107, pp. 459–462.

3. Kurzweg, U. H., 1986, "Temporal and Spatial Distribution of Heat Flux in Oscillating Flow Subjected to an Axial Temperature Gradient," Int. J. Heat Mass Transfer, 29, pp. 1969–1977.

4. Walsh, T. E., Yang, K. T., Nee, V. W., and Liao, Q. D., 1993, "Forced Convection Cooling in

5. Liao, Q. D., Yang, K. T., and Nee, V. W., 1995, "Enhanced Microprocessor Chip Cooling by Channeled Zero-Mean Oscillatory Air Flow," Advances in Electronic Packaging, Vol. 2, pp. 789–794.

6. Fusegi, T., 1996, "Mixed Convection in Periodic Open Cavities with Oscillatory Through flow,"Numer. Heat Transfer, Part A, 29, pp. 33–47.

7. P. C Chatwin, J. Fluid Mech. 71, 513 (1975)

8. U.H. Kurzweg, M.J. Jeager, Tuning effect in enhanced gas dispersion under oscillatory conditions, Physics of Fluids, 29 (4) (1986) 1324-1325.

9. E.J. Watson, Diffusion in oscillatory pipe flow, Journal of Fluid Mechanics, 133 (1983) 233-244.

10. M. J Jaeger and U.H Kurzweg, Phys. Fluid 26, 1380 (1983)

11. .G. I Taylor, Proc. R. Soc. London Ser. A22, 446 (1954)

12. R. Aris, "On the dispersion of Solute in a Fluid flowing through a Tube," Proc. R. Soc. London, Ser. A 235, 1956, pp 67

13. James D. Bozeman, Charles Dalton, 'Numerical Study of Viscous Flow in Cavity', Journal of Computational Physics, vol. 12, 1973.

14. USER GUIDE STAR-CCM+ Version 10.02.

15. PROFIR M. M., Mesh morphing implementation methods with examples, Proceedings of FG60, Bertinoro, Italy, June 16-19, 2010.

16. H. G. Harris, Jr. and S. L. Goren, "Axial Diffusion in a Cylinder with Pulsed Flow," Chemical Engineering Science, 1967, Vol. 22, pp. 1571 – 1576

17. A. Quarteroni and A. Valli. Numerical approximation of partial differential equations Springer, Berlin, 1994

18. PROFIR M. M., Mesh morphing techniques in CFD, Proceedings of ISCOPAM, Iasi, July 12-16, 2010.

19. FERZIGER, J.H., PERIC, M., Computational Methods for Fluid Dynamics, 3rd rev. ed., Springer-Verlag, Berlin, 2002

20. ALEXA M. Recent Advances in Mesh Morphing, Computer Graphics Forum (9/2002). BOER A., SCHOOT M.S., BIJL H., Mesh morphing based on radial function interpolation, Elsevier, 2007

21. R.A. Peattie, R. Budwig, Heat transfer in laminar, oscillatory flow in cylindrical and conical tubes, International Journal of Heat and Mass Transfer 32 (5) (1989) 923-934.

22. T. Inaba, M. Tahara, K. Saitoh, Longitudinal heat transfer in oscillatory flow in pipe bundles of various cross sections, JSME International Journal, 43 (3) (2000) 460-467.

Appendix A

Additional Figures
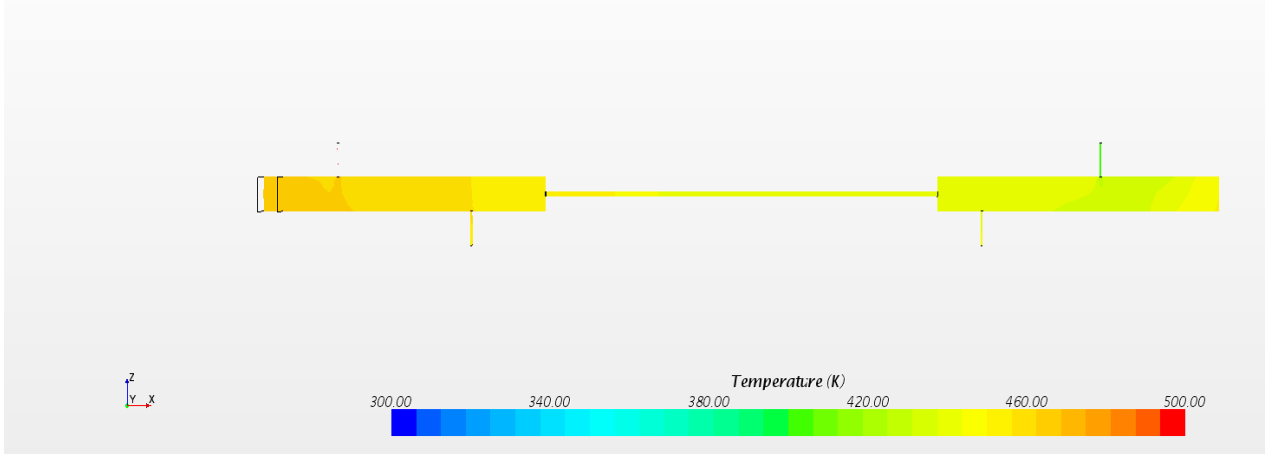
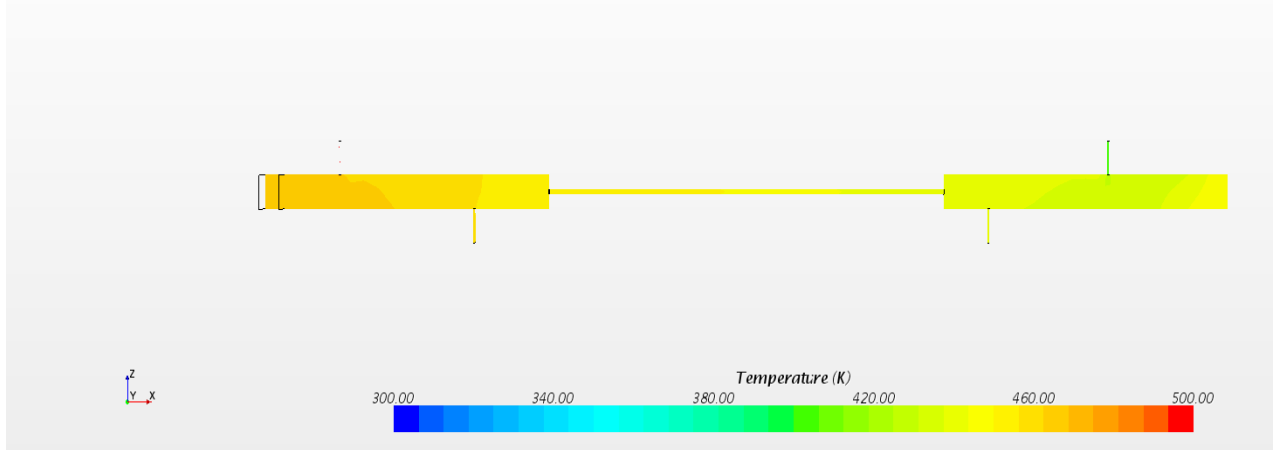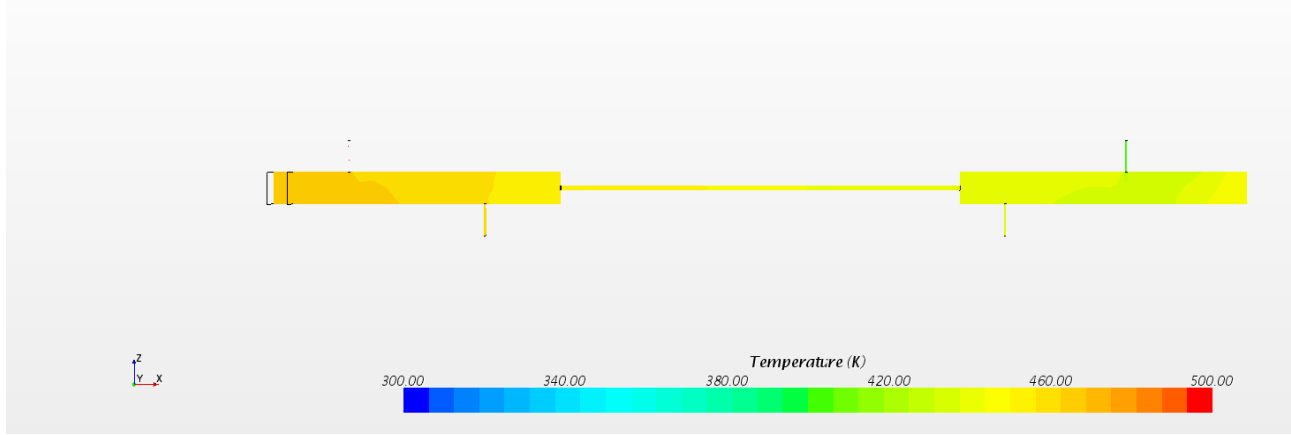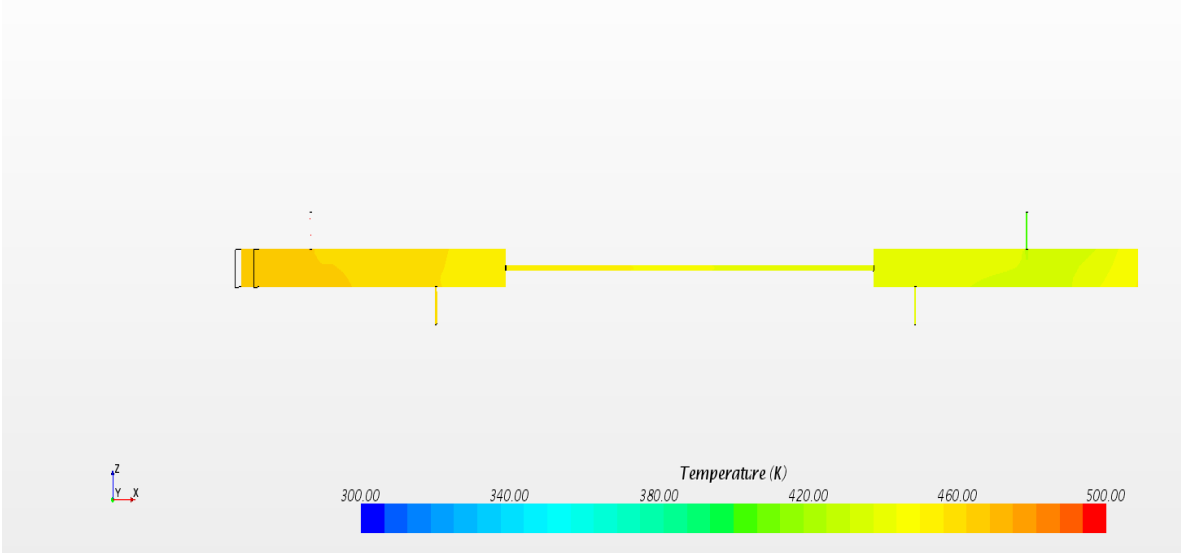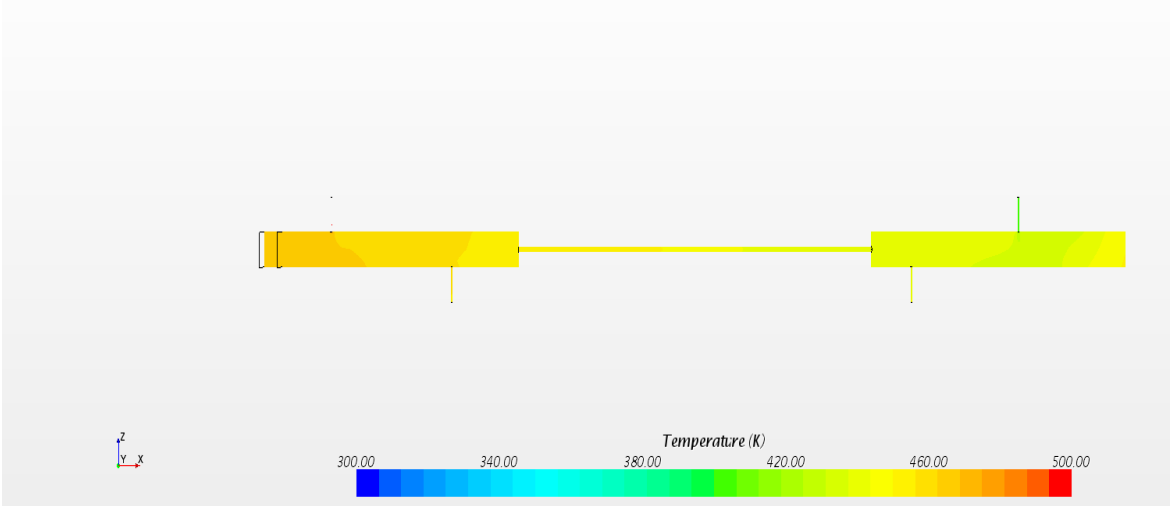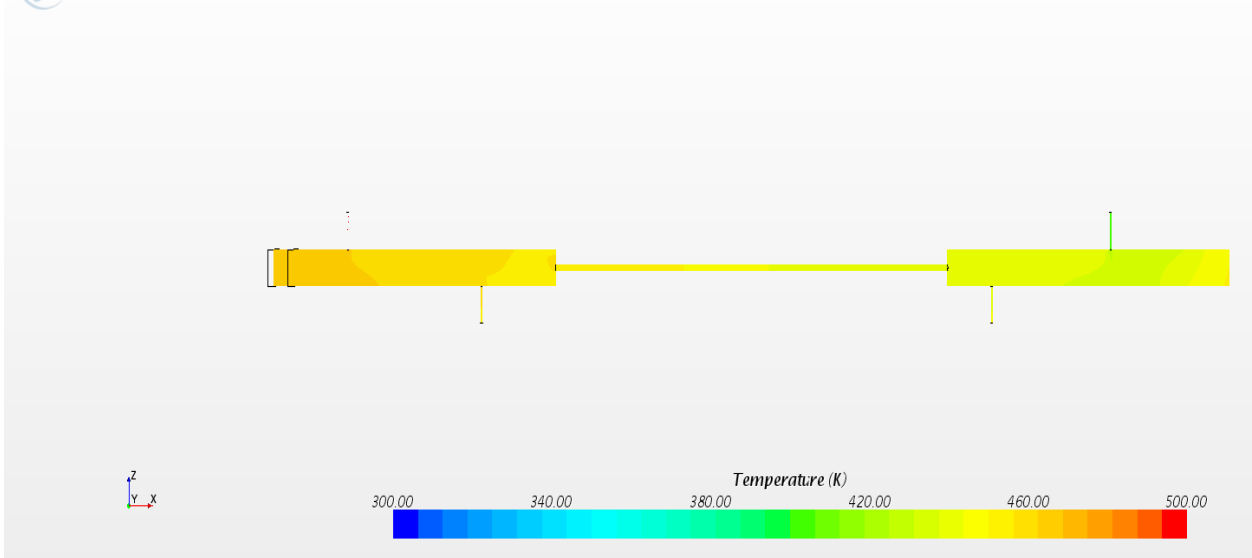*Figure 31: Diffusion of energy at 0.1 Hz*
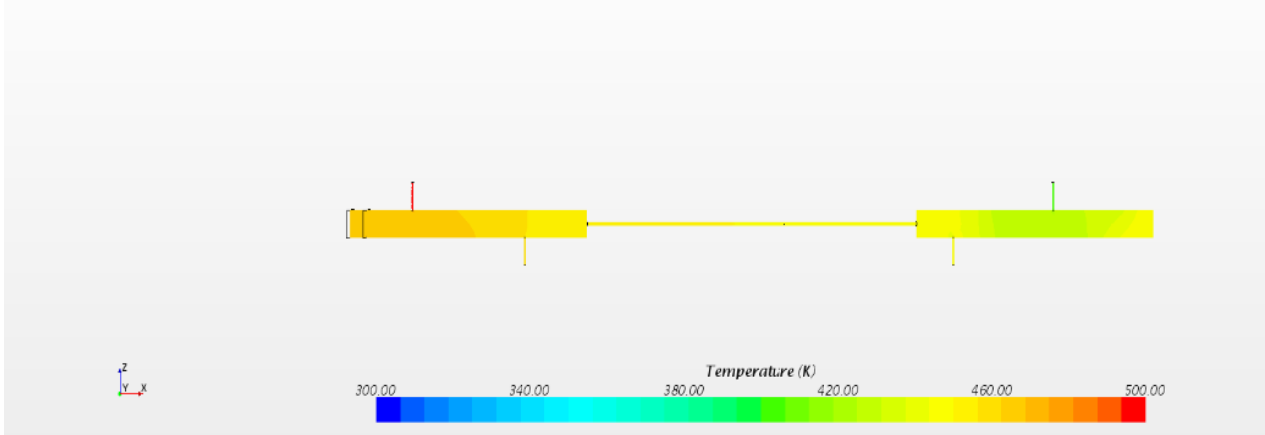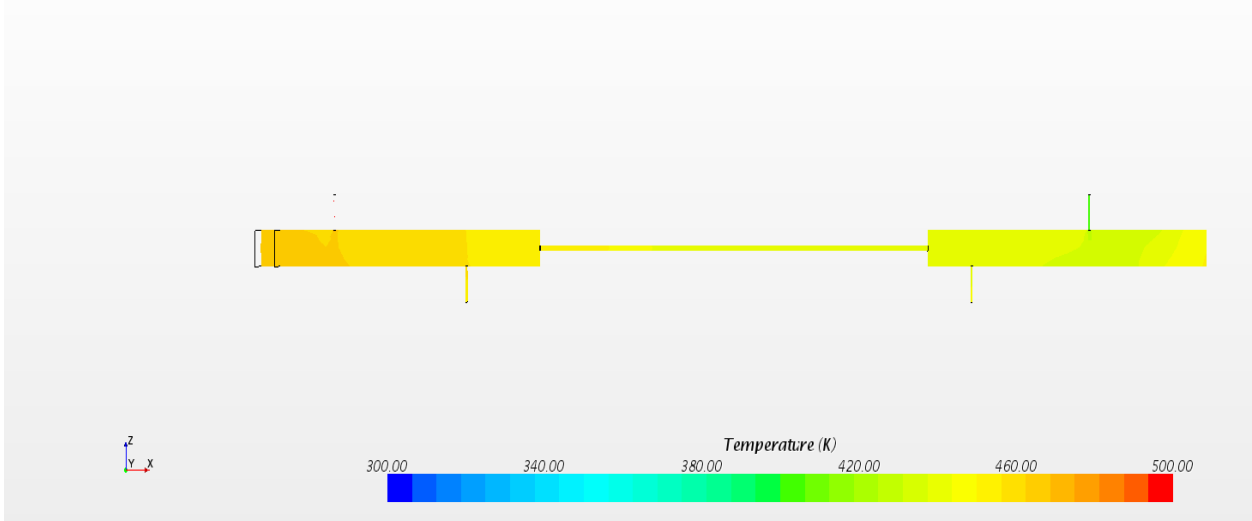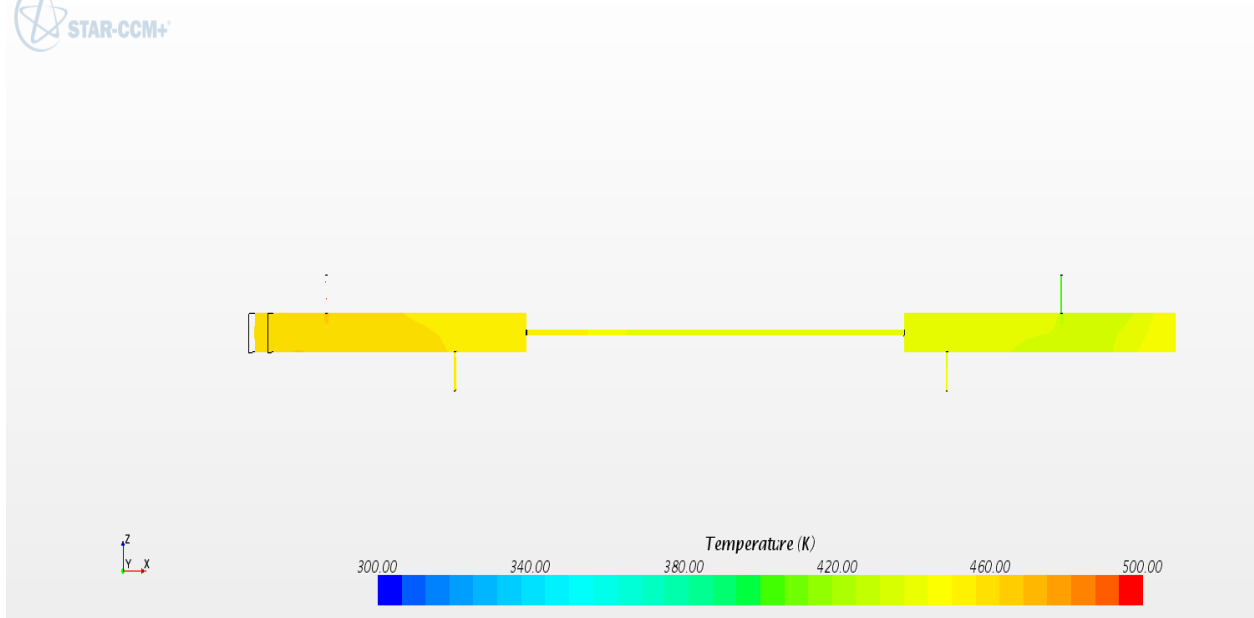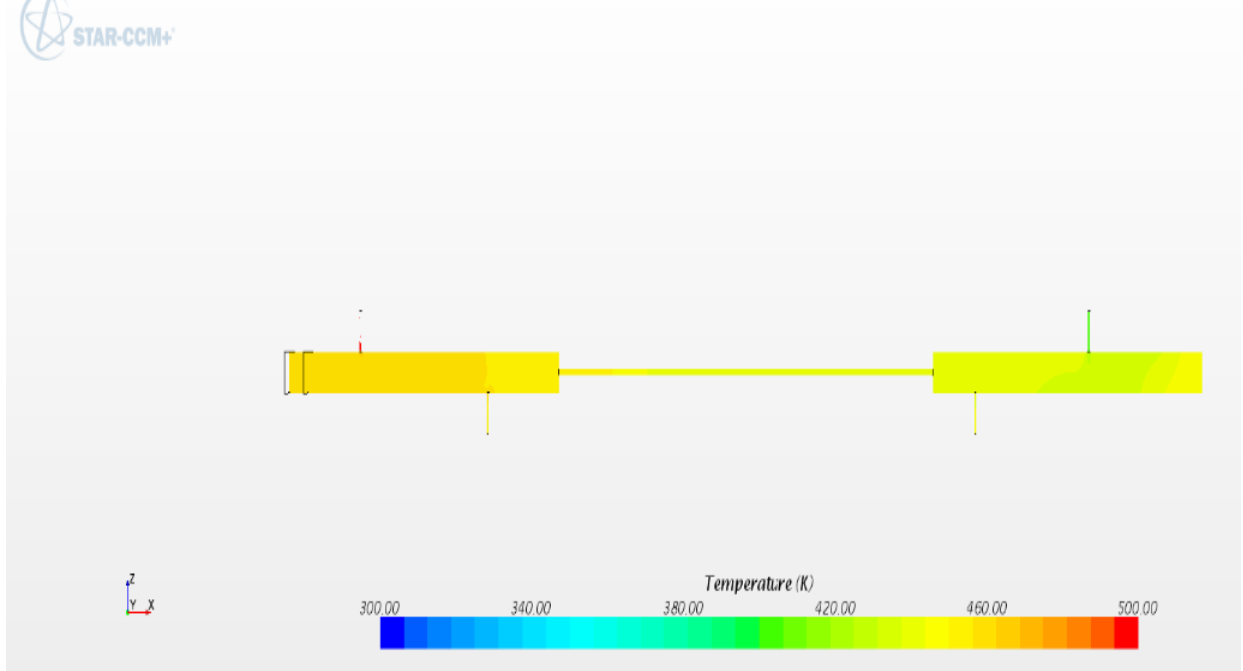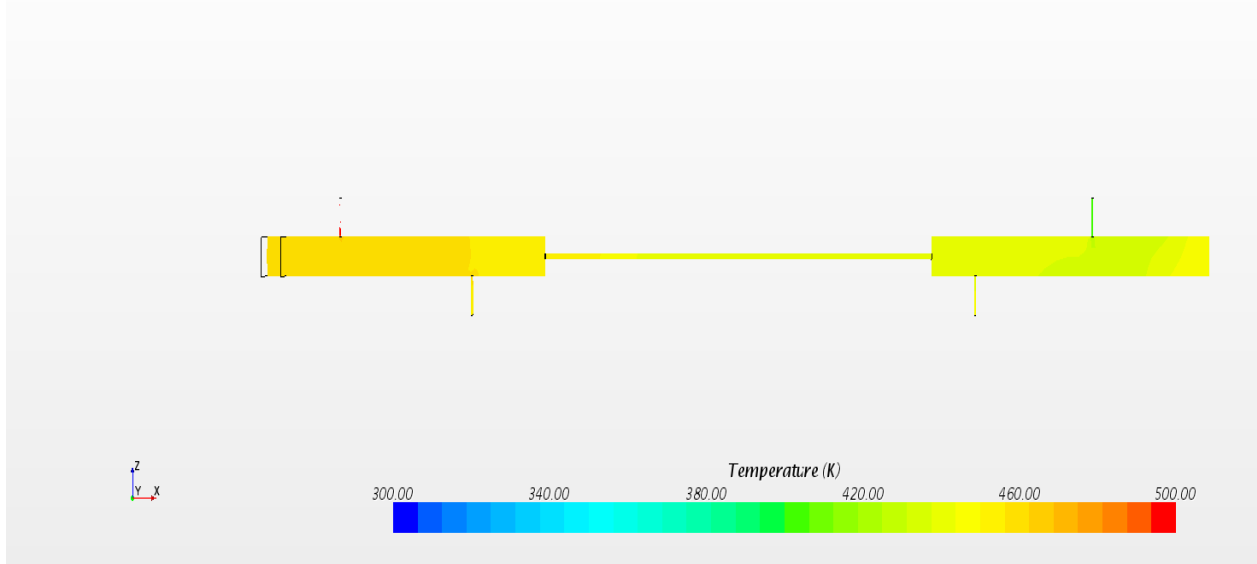

Figure 32: Diffusion of energy at 0.2 Hz
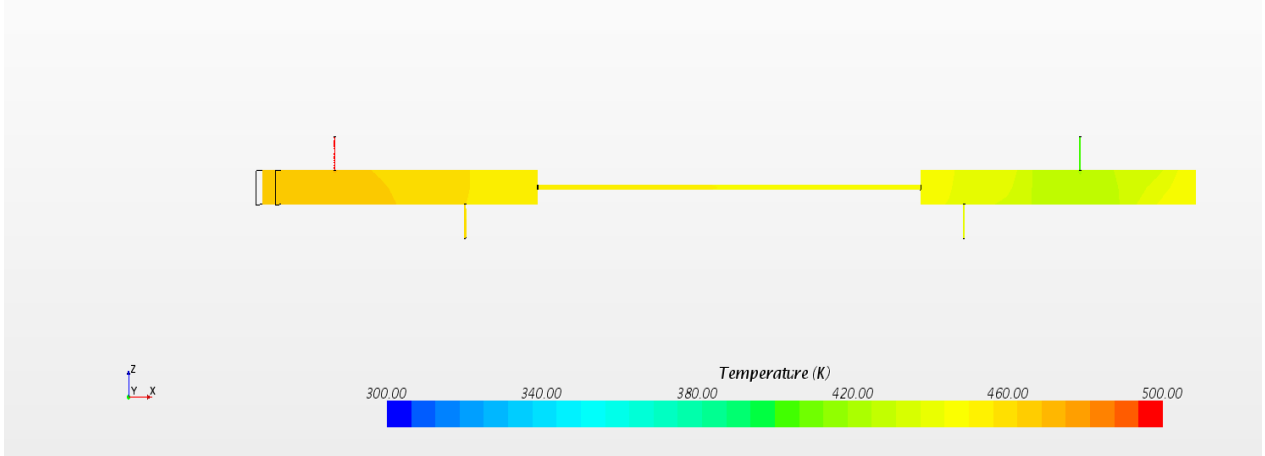
Figure 33: Diffusion of energy at 0.3 Hz
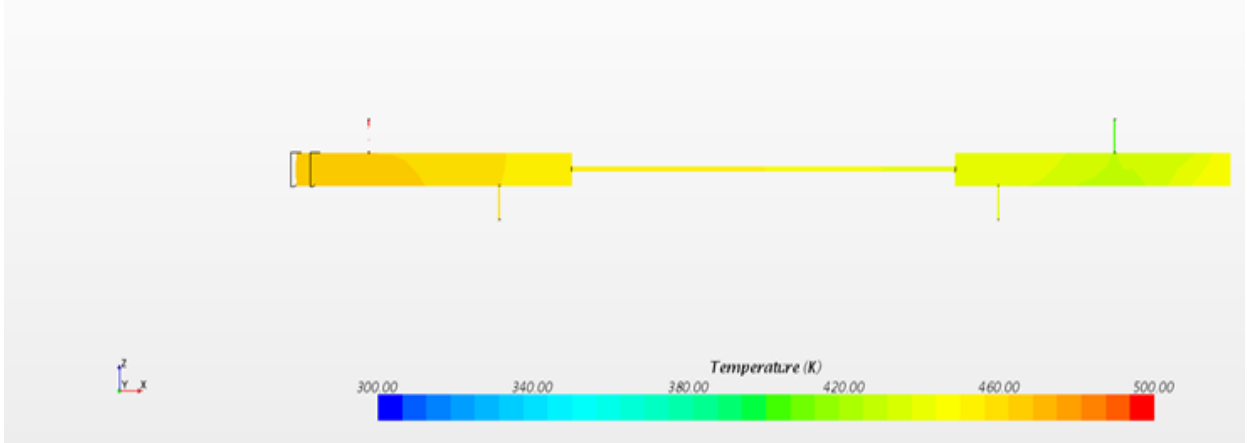
Figure 34: Diffusion of energy at 0.4 Hz

Figure 35: Diffusion of energy at 0.5 Hz

Figure 36: Diffusion of energy at 0.6 Hz

Figure 37: Diffusion of energy at 0.7 Hz

Figure 38: Diffusion of energy at 0.8 Hz

Figure 39: Diffusion of energy at 0.9 H

Figure 40: Diffusion of energy at 1 Hz

Figure 41: Diffusion of energy at 1.1 Hz

Figure 42: Diffusion of energy at 1.2 Hz
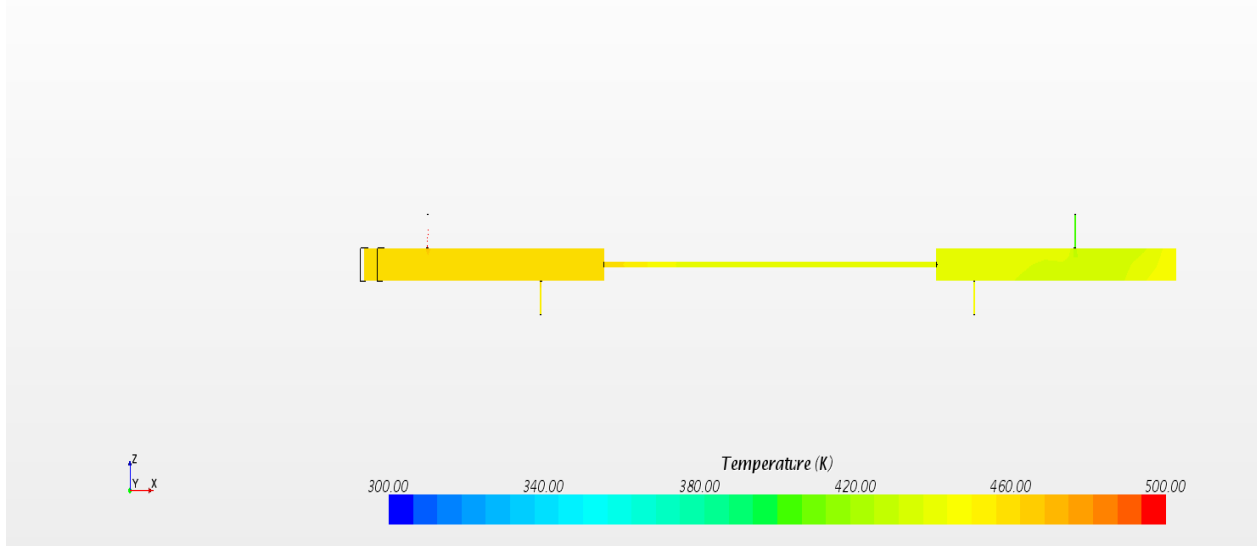
Figure 43: Diffusion of energy at 1.3 Hz

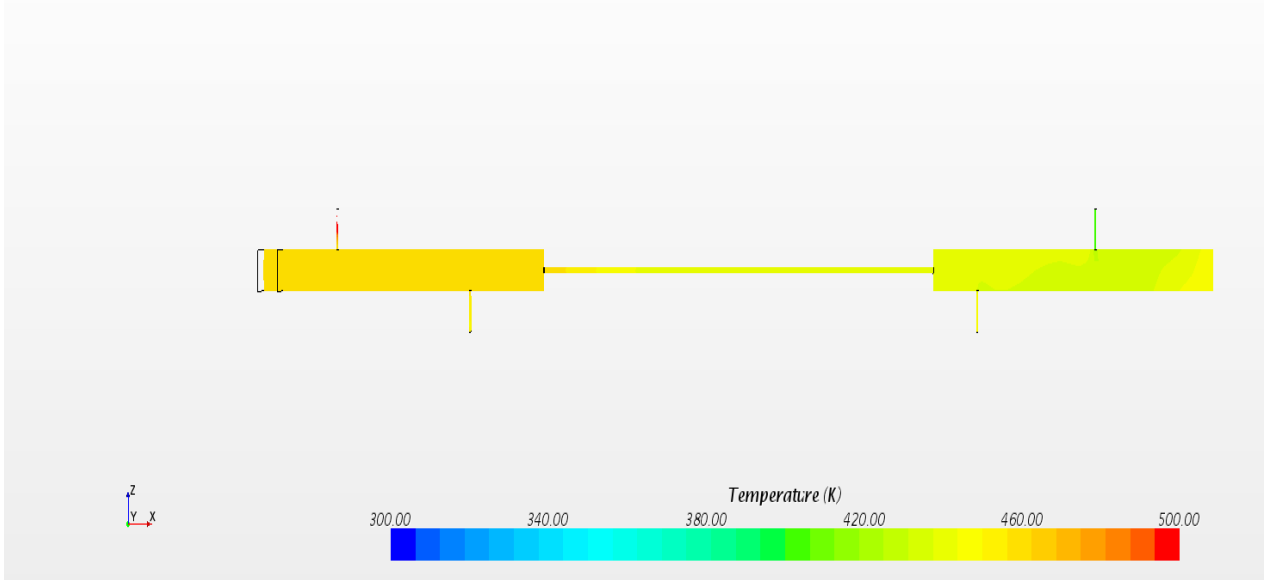*Figure 44: Diffusion of energy at 1.4 Hz*
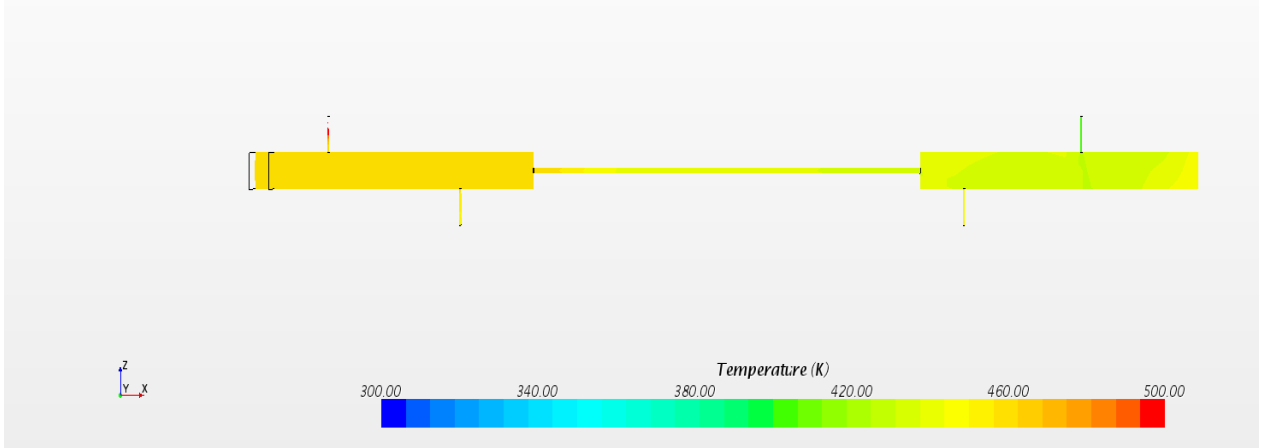
Figure 45: Diffusion of energy at 1.5 Hz

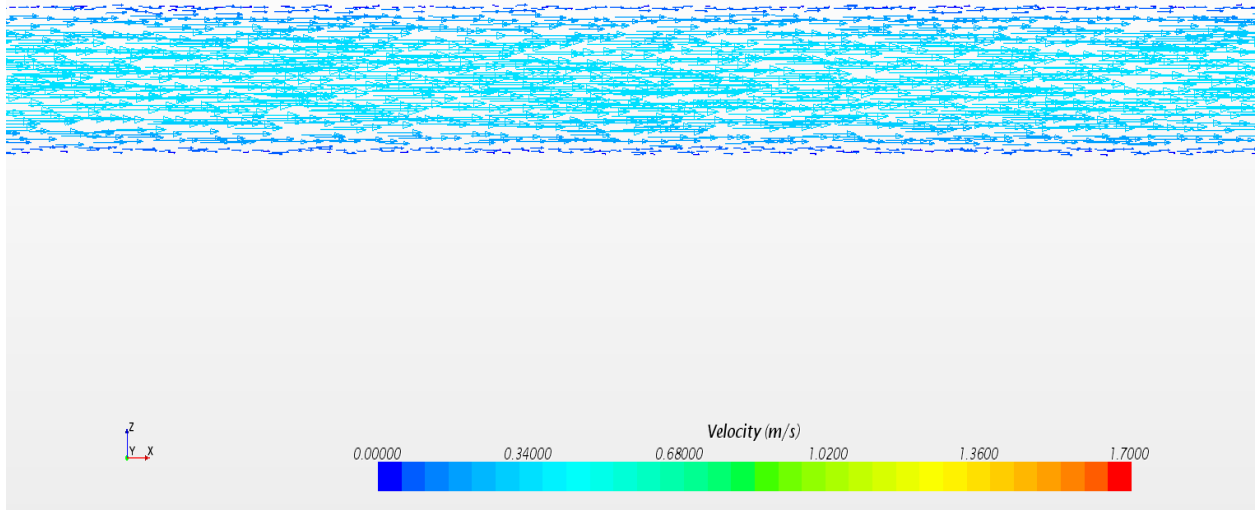Figure 46: Diffusion of energy at 1.6 Hz

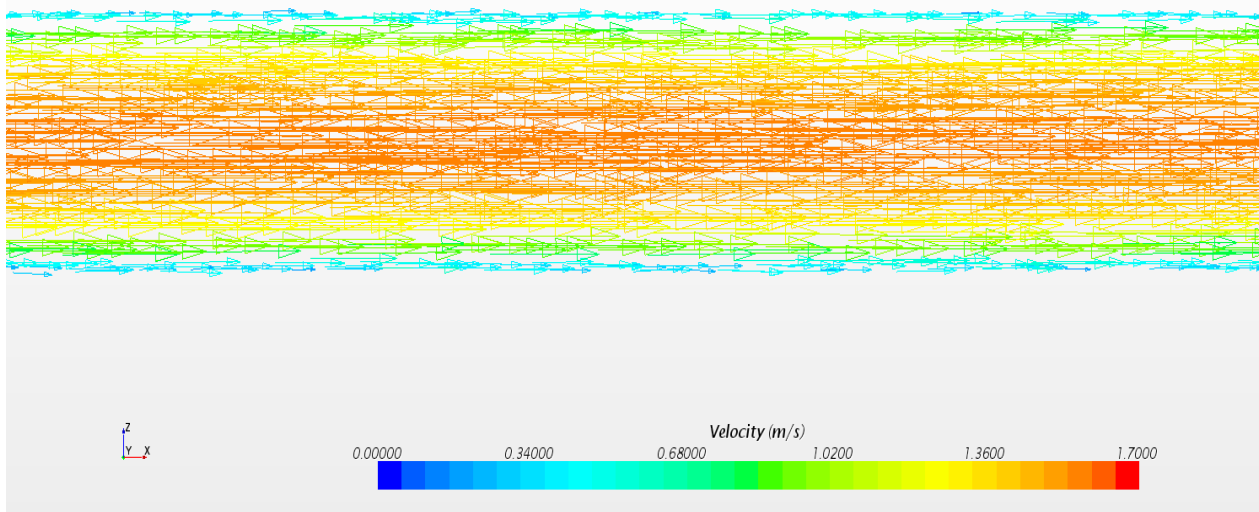*Figure 47: Velocity at 0.1 Hz*
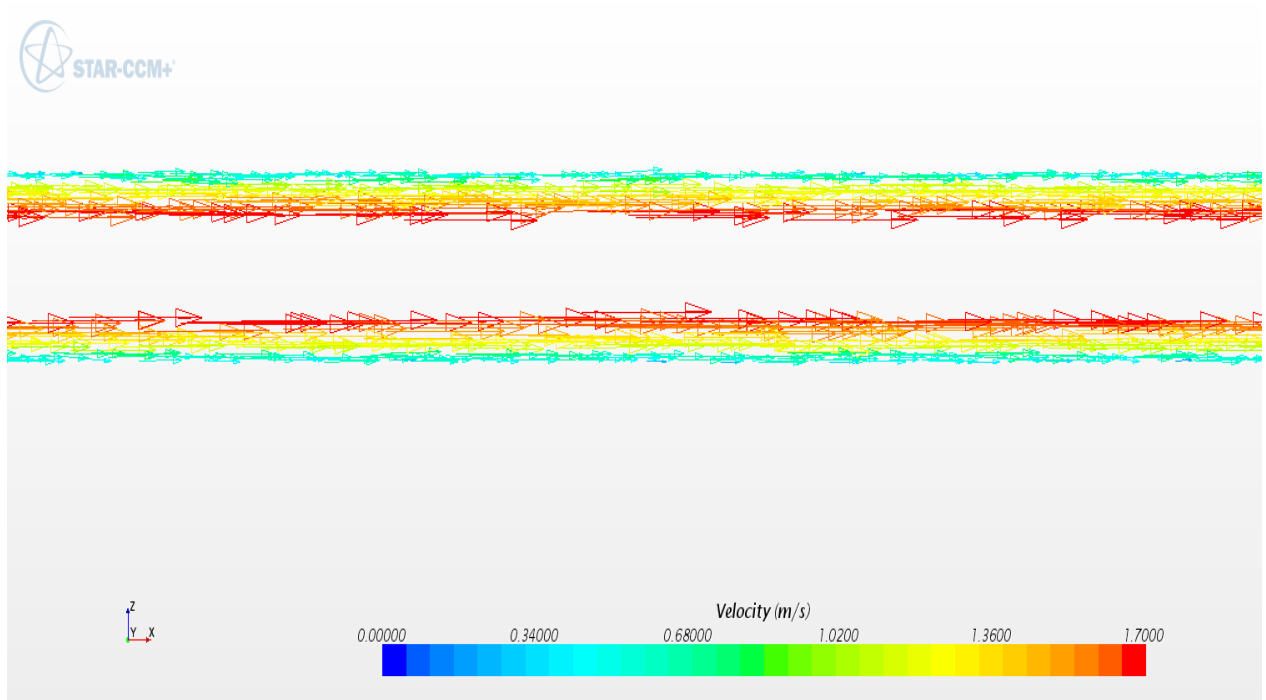

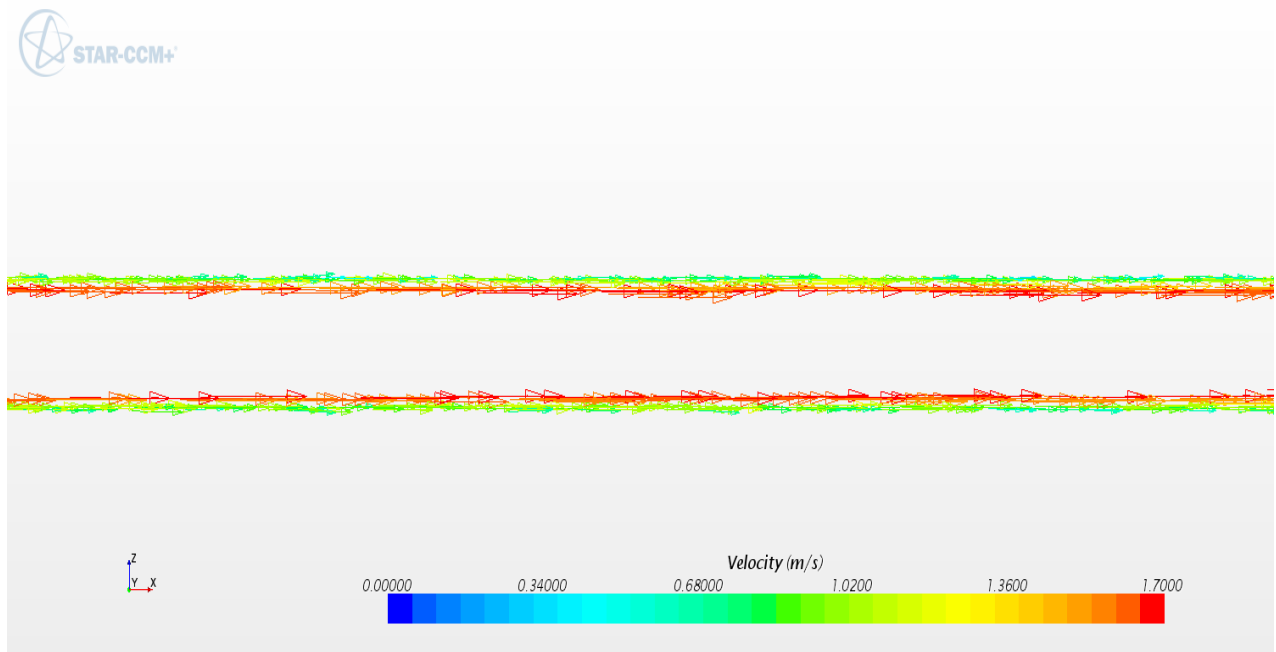*Figure 48: Velocity at 0.4 H*

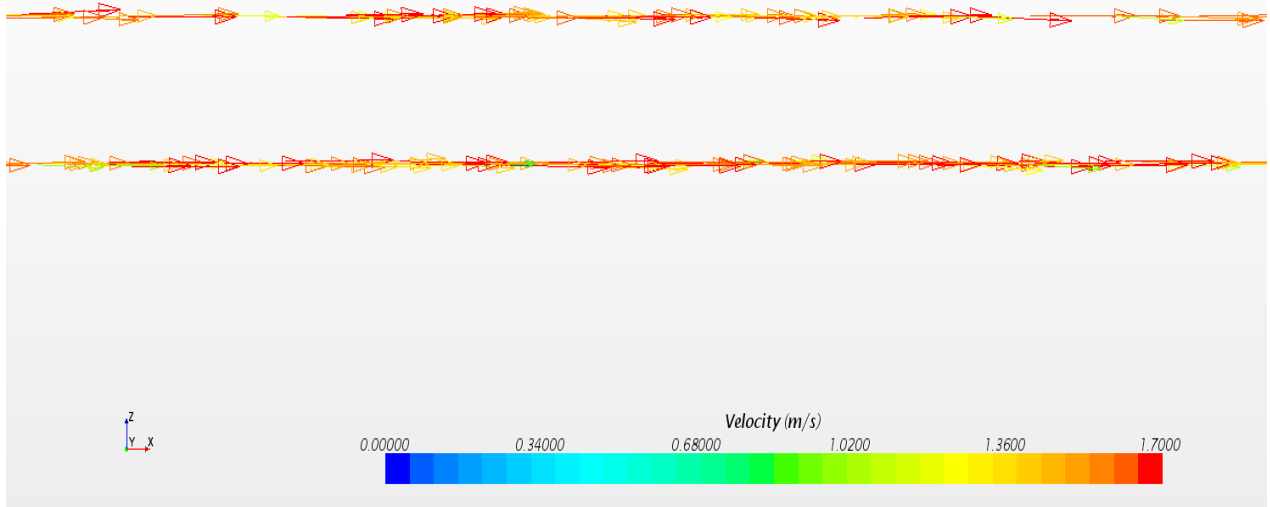*Figure 49: Velocity at 0.8 Hz*

Figure 50: Velocity at 1 Hz

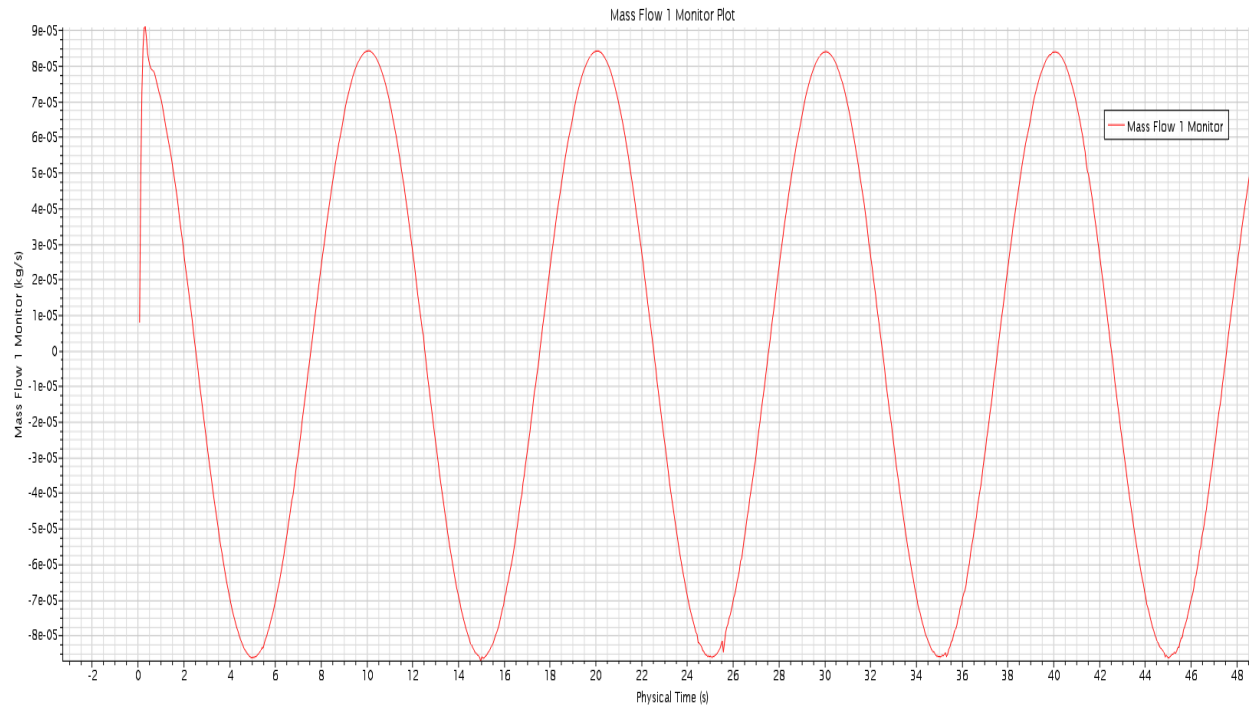*Figure 51: Velocity at 1.3 Hz*

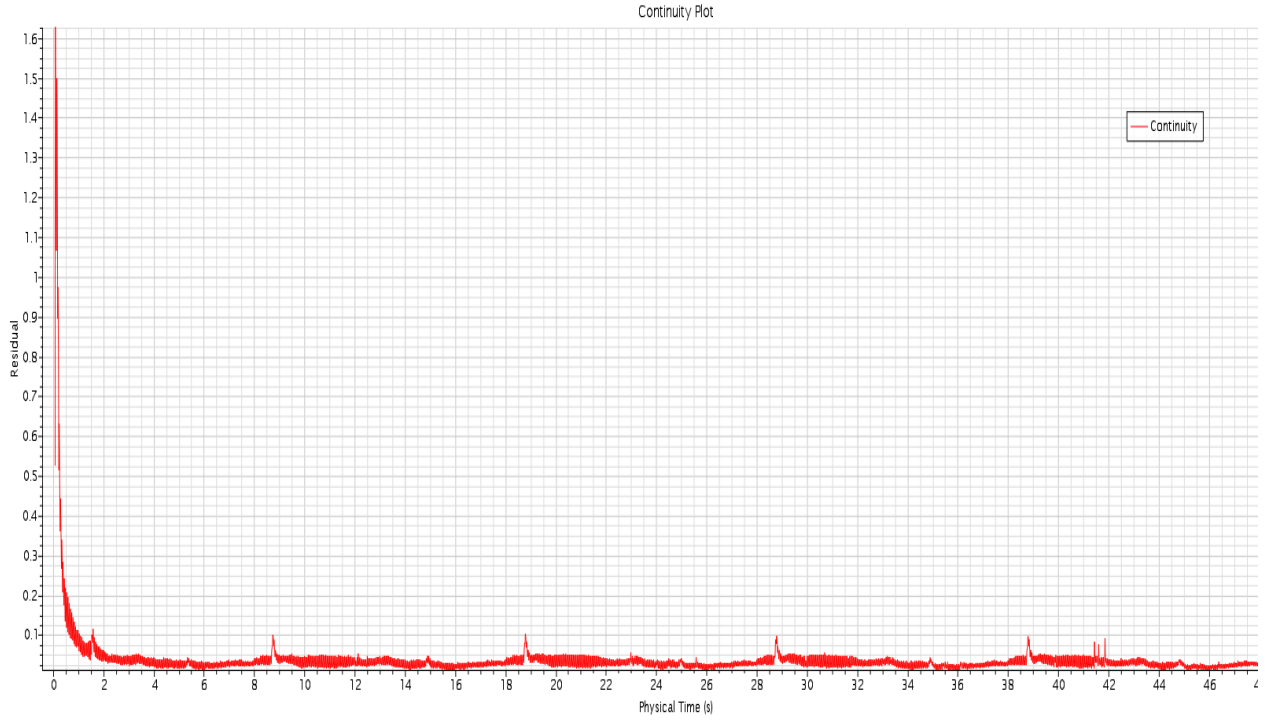Figure 52: Mass Flow Rate

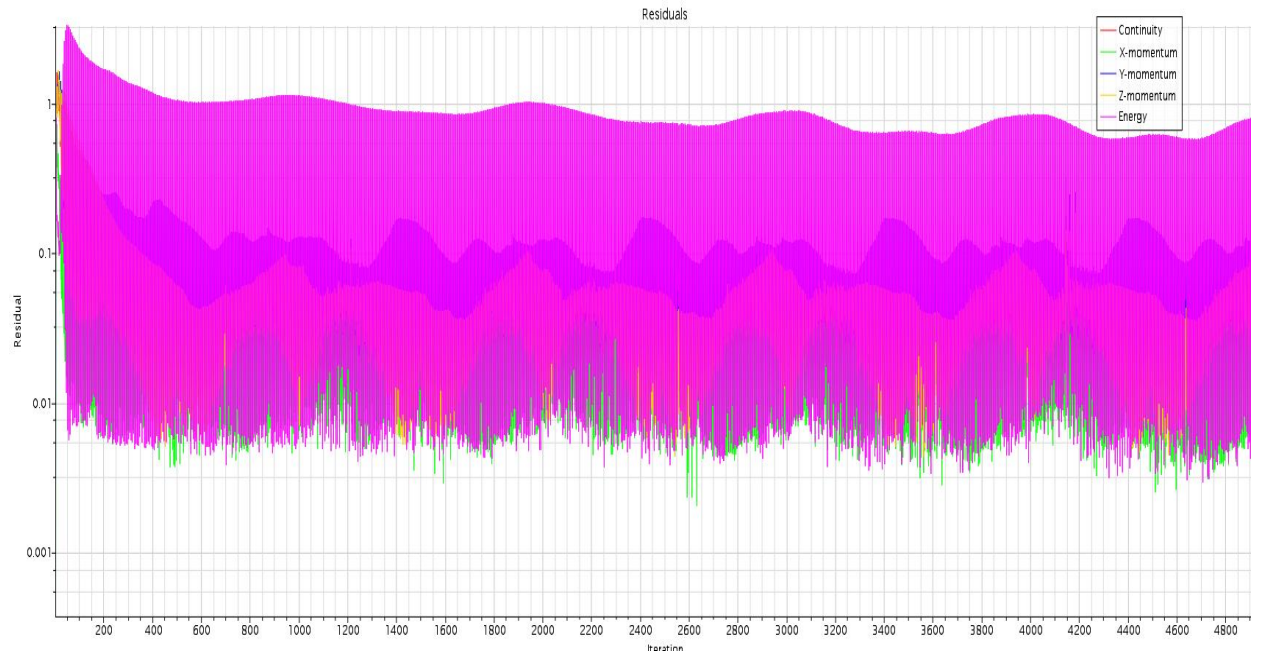Figure 53: Continuity of Unsteady state

Figure 54: Residual of Oscillation Flow

64
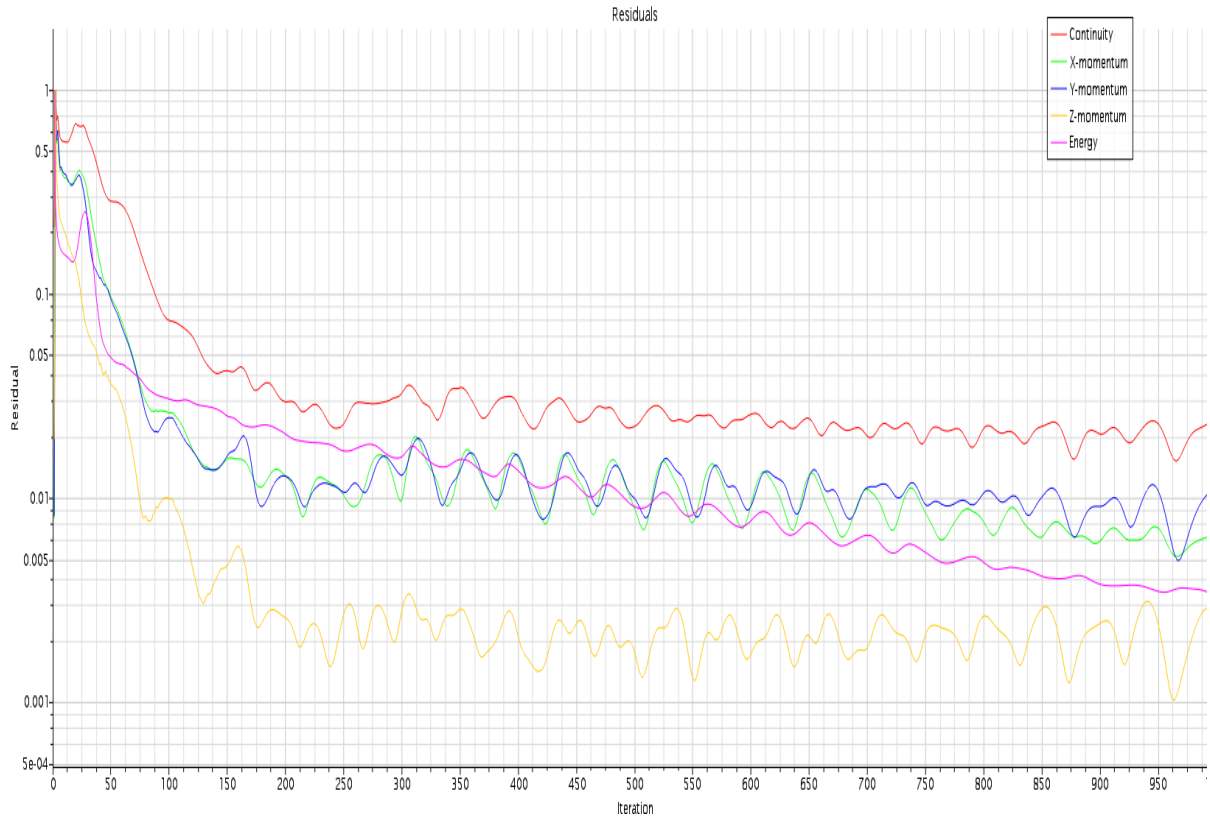
Figure 55: Residual of Steady State

65

Appendix B

Additional Tables

Table 4: results of temperature for case 1 with 5%L

Velocity=1.7m/s	Amplitude= 5%L			Time-step=0.05 s	
Case#	Frequency (HZ)	Temp. Inlet1 K	Temp. Out1 K	Temp. Inlet2 K	Temp.Out2 K
Case1	0.1	500	454.526	400	445.284
Case2	0.2	500	454.109	400	447.094
Case3	0.3	500	453.481	400	446.275
Case4	0.4	500	453.134	400	445.920
Case5	0.5	500	452.902	400	445.763
Case6	0.6	500	452.820	400	445.977
Case7	0.7	500	452.451	400	446.569
Case8	0.8	500	452.329	400	447.0.21
Case9	0.9	500	452.137	400	447.362
Case10	1	500	451.672	400	447.502
Case11	1.1	500	451.301	400	447.908
Case12	1.2	500	451.226	400	447.940
Case13	1.3	500	450.964	400	448.132
Case14	1.4	500	450.876	400	448.115
Case15	1.5	500	450.804	400	448.582
Case16	1.6	500	450.655	400	448.264

Table 5: Results of temperature for case 2 with 7%L

Velocity= 2.7 m/s		Amplitude=7%L		Time-step= 0.05s	
Case#	Frequency Hz	Temp. inlet1 K	Temp. Out1 K	Temp. Inlet2 K	Temp. Outlet2 K
Case1	0.1	500	454.196	400	446.250
Case2	0.2	500	453.741	400	446.448
Case3	0.3	500	453.141	400	445.785
Case4	0.4	500	452.788	400	445.872
Case5	0.5	500	451.707	400	448.002
Case6	0.6	500	452.459	400	446.447
Case7	0.7	500	451.775	400	447.282
Case8	0.8	500	451.463	400	447.624
Case9	0.9	500	451.516	400	447.873
Case10	1	500	451.411	400	448.072
Case11	1.1	500	451.351	400	448.410
Case12	1.2	500	450.894	400	448.522
Case13	1.3	500	450.033	400	448.809
Case14	1.4	500	450.026	400	448.842
Case15	1.5	500	450.033	400	448.612
Case16	1.6	500	450.026	400	448.624

Table 6: Results of temperature for case 3 with 10%L

Velocity=1.7m/s		Amplitude=10%L		Time-step= 0.05 s	
Case#	Frequency	Temp.inlet1 (K)	Temp. outlet 1 (K)	Temp.inlet2 (K)	Temp. outlet 2 (K)
Case1	0.1	500	454.196	400	446.250
Case2	0.2	500	453.741	400	446.448
Cae3	0.3	500	453.141	400	445.785
Case4	0.4	500	452.788	400	445.872
Case5	0.5	500	451.707	400	448.002
Case6	0.6	500	452.549	400	446.474
Case7	0.7	500	452.313	400	447.282
Case8	0.8	500	451.99	400	447.624
Case9	0.9	500	451.757	400	447.949
Case10	1	500	451.463	400	447.873
Case11	1.1	500	451.516	400	448.072
Case12	1.2	500	451.411	400	448.410
Case13	1.3	500	451.351	400	448.522
Case14	1.4	500	450.894	400	448.809
Case15	1.5	500	450.033	400	448.842
Case16	1.6	500	450.026	400	448.612